

Neoadjuvant triplet immune checkpoint blockade in newly diagnosed glioblastoma

Received: 24 July 2024

Accepted: 14 January 2025

Published online: 27 February 2025

 Check for updates

A list of authors and their affiliations appears at the end of the paper

Glioblastoma (GBM) is an aggressive primary adult brain tumor that rapidly recurs after standard-of-care treatments, including surgery, chemotherapy and radiotherapy. While immune checkpoint inhibitor therapies have transformed outcomes in many tumor types, particularly when used neoadjuvantly or as a first-line treatment, including in melanoma brain metastases, they have shown limited efficacy in patients with resected or recurrent GBM. The lack of efficacy has been attributed to the scarcity of tumor-infiltrating lymphocytes (TILs), an immunosuppressive tumor microenvironment and low tumor mutation burden typical of GBM tumors, plus exclusion of large molecules from the brain parenchyma. We hypothesized that upfront neoadjuvant combination immunotherapy, administered with disease in situ, could induce a stronger immune response than treatment given after resection or after recurrence. Here, we present a case of newly diagnosed IDH-wild-type, *MGMT* promoter unmethylated GBM, treated with a single dose of neoadjuvant triplet immunotherapy (anti-programmed cell death protein 1 plus anti-cytotoxic T-lymphocyte protein 4 plus anti-lymphocyte-activation gene 3) followed by maximal safe resection 12 days later. The anti-programmed cell death protein 1 drug was bound to TILs in the resected GBM and there was marked TIL infiltration and activation compared with the baseline biopsy. After 17 months, there is no definitive sign of recurrence. If used first line, before safe maximal resection, checkpoint inhibitors are capable of immune activation in GBM and may induce a response. A clinical trial of first-line neoadjuvant combination checkpoint inhibitor therapy in newly diagnosed GBM is planned (GIANT; trial registration no. [NCT06816927](https://clinicaltrials.gov/ct2/show/study/NCT06816927)).

Glioblastoma (GBM) is the most aggressive form of adult-type diffuse glioma and is characterized by the absence of *IDH1* and *IDH2* mutations¹. Standard therapy, of maximal safe resection followed by radiotherapy and temozolomide chemotherapy (the Stupp protocol²), provides a 2.5-month median overall survival (OS) benefit over surgery with radiotherapy alone in unselected IDH-agnostic patients with GBM². Patients with *MGMT* promoter-unmethylated GBM have the worst outcomes, with a median OS of 14.1 months despite standard-of-care chemoradiotherapy³. Most patients will die within the first 2 years of diagnosis³.

Immune checkpoint inhibitors (ICIs) have revolutionized the management of many cancer types, including melanoma, where the 10-year melanoma-specific survival rate has increased from less than 5% to 52% of patients in stage IV treated with combination ICIs⁴. In randomized GBM trials, adjuvant anti-programmed cell death protein 1 (PD-1) administered in combination with radiotherapy (plus temozolomide in methylated GBM) after maximal safe resection and followed by anti-PD-1 monotherapy to 12 months, showed no benefit over the standard Stupp protocol^{5–7}. The lack of ICI activity in GBM is thought

✉ e-mail: georgina.long@sydney.edu.au

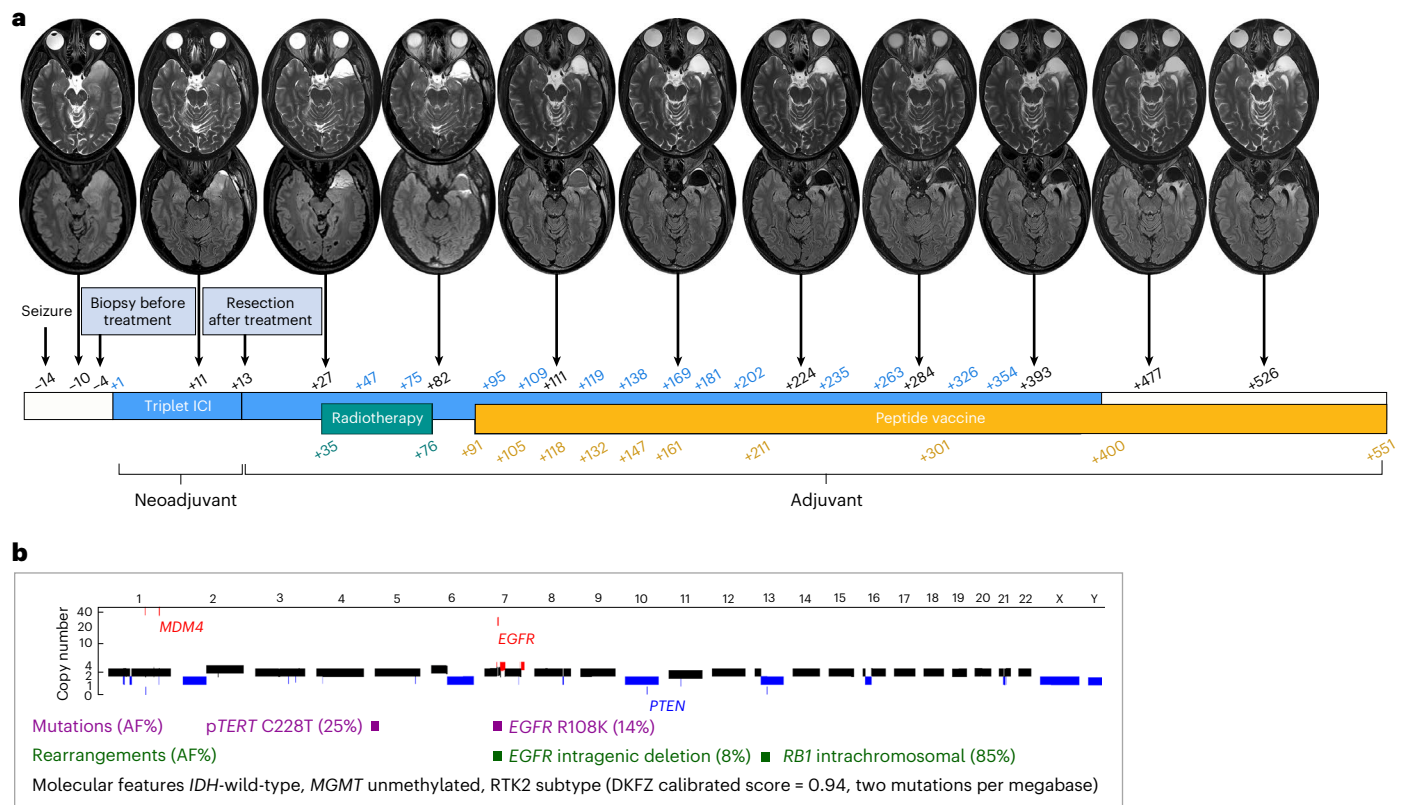


Fig. 1 | Clinical and molecular details of the patient with GBM and treatment regimen. **a**, Serial magnetic resonance imaging scans with gadolinium including T2-weighted (top) and fluid-attenuated inversion recovery sequences (bottom) shown during the treatment schedule. The treatment time points, relative to neoadjuvant ICI therapy initiation (day +1) are shown, including ICI cycles (blue), radiotherapy (green) and peptide vaccine doses (yellow). The peptide vaccine program was recently completed, and ongoing analyses will be reported separately. The most recent scan (day +526) demonstrated grossly stable postsurgical changes with persistent white matter T2 fluid-attenuated inversion recovery hyperintensity in the left temporal periventricular white matter posterior to the temporal pole surgical bed and the left temporal operculum. There was a stable small focus of enhancement lateral to the left

temporal horn. These changes were all within the high-dose radiotherapy field. No focal hyperperfusion or diffusion restriction to suggest recurrent disease was observed. **b**, Key genomic events identified in pretreatment GBM. Segment-level copy number profile across chromosomes includes amplifications in red (copy number > 2.5) and deletions in blue (copy number < 1.5). Copy number-neutral regions are shown in black. For copy number, the y axis is shown in pseudo-logarithmic scale. Somatic mutations (magenta) and rearrangements (dark green) of potential clinical significance or in known cancer genes are included in the genomic region where each gene resides together with their allele fraction (AF). All events were identified based on the WGS of the pretreatment (day -4) tumor specimen, except for the *EGFR* (R108K) mutation identified based on the WGS of the resection (posttreatment; day +13) specimen.

to reflect a low tumor mutational burden (TMB) and an immunosuppressive tumor microenvironment (TME) characterized by abundant microglia and macrophages, a scarcity of tumor-infiltrating lymphocytes (TILs) and immature natural killer cells^{8,9}.

Neoadjuvant ICI outperforms adjuvant delivery in many cancer types but has only been tested using single-agent anti-PD-1 in small numbers of heavily pretreated (corticosteroids and chemoradiotherapy) patients with recurrent GBM¹⁰⁻¹³ (Extended Data Table 1). In these patients, neoadjuvant PD-1 blockade promoted the activation of TILs¹⁰⁻¹² and extended OS (13.7 months with neoadjuvant ICI versus 7.5 months with adjuvant)¹¹. Notably, two of three newly diagnosed patients with GBM who received neoadjuvant anti-PD-1 before maximal safe resection remained disease free for more than 33 and 28 months, respectively¹². Response to neoadjuvant immunotherapy may be supported by the presence of tumor-associated effector CD8⁺ T cells identified in the cranial bone marrow of treatment-naïve, newly diagnosed patients with GBM¹⁴.

Here, we describe a case study of a newly diagnosed patient with GBM (IDH-wild-type, unmethylated *MGMT* promoter) treated with triplet neoadjuvant ICI upfront (nivolumab, anti-PD-1; ipilimumab, anti-cytotoxic T-lymphocyte protein 4 (CTLA-4); and relatlimab, anti-lymphocyte-activation gene 3 (LAG3)), before maximal safe resection. Triple ICI therapy was selected based on an unprecedented survival

in the phase I trial in advanced melanoma¹⁵, as well as the significantly superior activity of the combination of multiple ICIs versus ICI monotherapy in melanoma with a poor TME^{16,17} (low CD8⁺ T cells, low TMB and low interferon- γ (IFN γ)), metastases to the brain¹⁸ or primary resistance to anti-PD-1 therapy¹⁹—all features found in GBM. Our findings confirm the urgent need to investigate this strategy in clinical trials.

Patient and GBM characteristics

A previously well 56-year-old male presented with new-onset generalized seizure and no prior symptoms (pre-ICI treatment, day -14). After initial management (Supplementary Results 1), the patient was diagnosed with a left temporal lobe GBM (IDH-wild-type, central nervous system WHO grade 4, RTK2 subtype (DKFZ calibrated score = 0.94)) after an open craniotomy biopsy (pre-ICI treatment, day -4; Fig. 1a). The tumor was a pleomorphic, mitotically active, diffusely infiltrative astrocytic glioma with negative IDH1 (R132H) immunohistochemistry (IHC) and retained nuclear ATRX stain. Mitoses were present at up to 8–10 per ten high-power fields (field diameter = 0.58 mm). There was no evidence of microvascular proliferation or necrosis (Supplementary Results 2). Pyrosequencing revealed a *TERT* promoter mutation (C228T) and confirmed no *IDH1* codon 132 or *IDH2* codon 172 mutation. The tumor was unmethylated at the *MGMT* promoter region. Moderate-to-strong p53 nuclear staining was observed in tumor cells.

Microsatellite status was stable. Whole-genome sequencing (WGS) (mean coverage = 85X) revealed focal amplification of the *EGFR* and *MDM4* genes, homozygous *PTEN* deletion and inactivating rearrangement of *RBI* with a low TMB (two mutations per megabase; Fig. 1b and Extended Data Table 2).

The patient's Eastern Cooperative Oncology Group Performance Status fluctuated between 0 and 1 because of postictal symptoms, surgery and lumbar punctures in the initial 4 weeks after presentation. In the 2 weeks before the initiation of treatment, there was no evidence of tumor growth or peritumoral edema on imaging. Corticosteroids were not commenced at any time point.

Neoadjuvant combined (triplet) ICI and outcomes

After treatment with intravenous neoadjuvant triplet ICI on day +1 (cycle 1: nivolumab 480 mg plus relatlimab 160 mg plus ipilimumab 80 mg), the patient underwent safe maximal resection (day +13; Supplementary Results 3), a 6-week course of adjuvant radiotherapy from day +35 (60 Gy in 30 fractions), adjuvant ICI from day +47 and adjuvant personalized peptide vaccination from day +91 (Fig. 1 and Extended Data Table 3). Adjuvant ICIs were administered as monotherapy or in combination, depending on toxicity and with avoidance of corticosteroids (grade 1 (and after cycle 12, grade 3) hepatitis, grade 1 conjunctivitis and grade 1 dermatitis attributed to ipilimumab). Circulating tumor cells (CTCs) (4',6-diamidino-2-phenylindole (DAPI) + glial fibrillary acidic protein (GFAP) + epidermal growth factor receptor (EGFR) + CD45⁺ CD66b⁺) zero-converted after therapy (16 CTCs in 7.5 ml blood detected on day -9 versus zero CTCs on day +190; Extended Data Fig. 1). At the last radiographic assessment (day +526, 17 months), there was no definitive evidence of recurrence (Fig. 1a).

Neoadjuvant ICI reshapes the GBM immune landscape

Chromogenic IHC and high-plex immunofluorescence of pretreatment (day -4) and posttreatment (day +13) formalin-fixed paraffin-embedded tumor specimens confirmed increases in the number of CD3⁺ T cells (Fig. 2a,b), including CD3⁺CD4⁺ T cells (greater than tenfold increase in the posttreatment specimen relative to pretreatment (from 0.3% to 5%)) and CD3⁺CD8⁺ cytotoxic T cells (eightfold increase posttreatment relative to pretreatment (from 0.4% to 3%); Fig. 2b). To account for potential localized inflammation induced by the initial biopsy, we confirmed a global increase in infiltration of CD3⁺ T cells via chromogenic IHC across all posttreatment tumor sections analyzed from the left temporal and amygdala regions (up to 30 mm from the biopsy site), compared with the pretreatment biopsy tissue (Extended Data Fig. 2). This contrasted with our findings in a resection sample from a separate patient with an untreated right frontal GBM, showing only a very localized T cell infiltrate due to the diagnostic biopsy performed 14 days before the resection (nearly zero T cells 8 mm from the biopsy site; Extended Data Fig. 2). High-dimensional-spatial phenotyping of formalin-fixed paraffin-embedded GBM specimens revealed increased colocalization of CD4⁺ and CD8⁺ T cells with tumor cells, and a notable

decrease in the colocalization of macrophages and microglial cells with tumor cells in response to neoadjuvant ICI treatment (Fig. 2b).

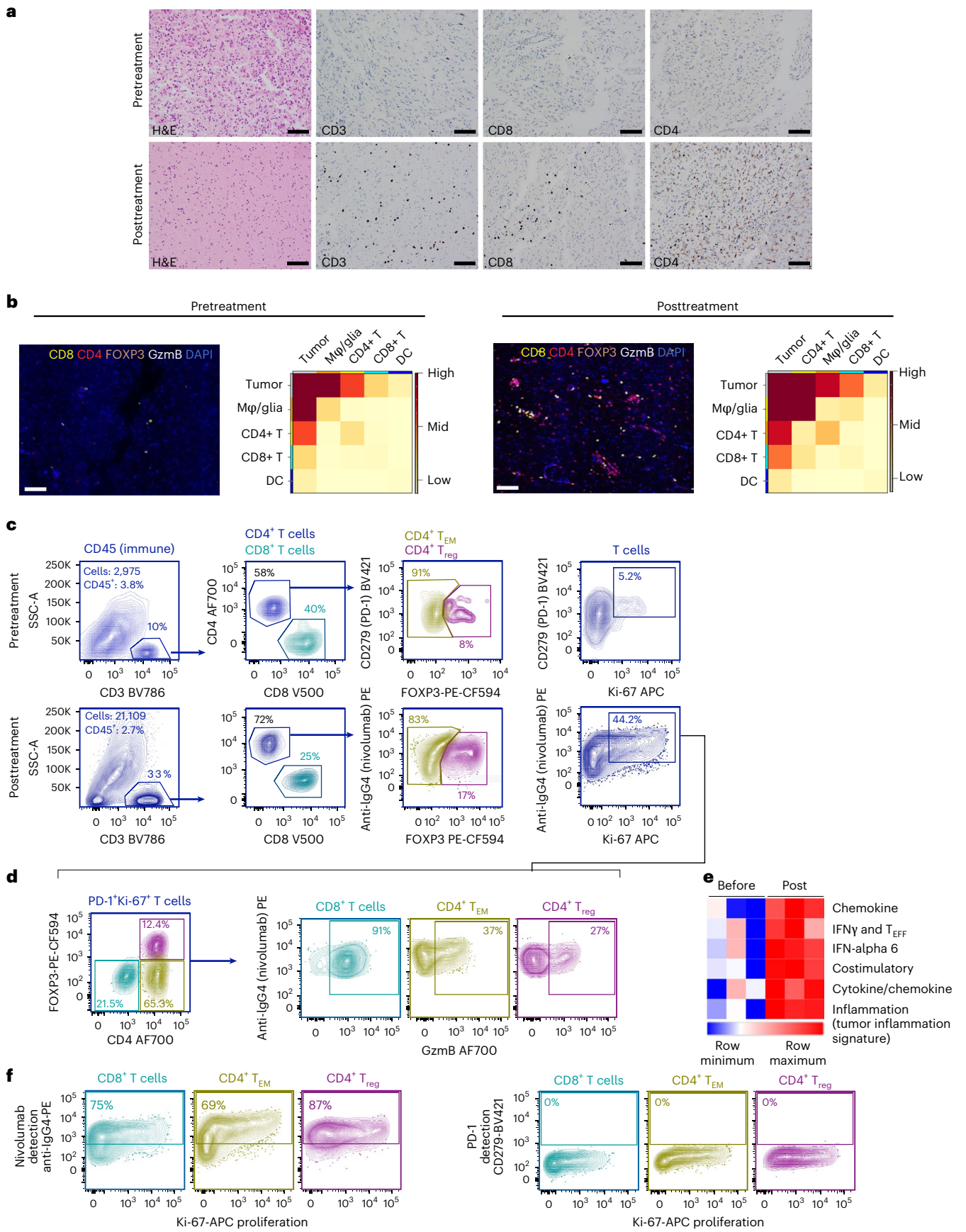
Multiparameter flow cytometry analysis was performed on the freshly dissociated pretreatment and posttreatment GBM specimens, and on an unrelated series of 11 primary GBM tumors resected from patients undergoing their first surgery. The CD45⁺ immune cell content in the 12 pretreatment GBMs ranged from 0.4% to 34.0% of the total viable cell population (median = 8.7%; Extended Data Fig. 3). The frequency of tumor-infiltrating CD3⁺ (range = 3–23%; median = 9.5%), CD4⁺FOXP3⁻ effector memory (T_{EM}) (range = 1–12%; median = 3.2%), CD4⁺FOXP3⁺ regulatory T (T_{reg}) cells (range = 0–2.5%; median = 0.3%) and CD8⁺ T cells (range = 1–9%; median = 4.3%) were also variable in the pretreatment GBM specimens (Extended Data Fig. 3). After ICI treatment, the posttreatment GBM specimen showed a marked increase in the relative proportion of T cells, with CD3⁺ T cells rising from 9.8% to 32.7%, CD4⁺ T_{EM} cells from 5.1% to 19.0%, CD4⁺ T_{reg} cells from 0.4% to 4.5% and CD8⁺ T cells from 3.9% to 8.2% (Extended Data Fig. 3). When compared with 31 pretreatment primary GBM tumors (12 from this study and 19 from a published series²⁰), the ICI-treated posttreatment GBM specimen had the highest proportion of infiltrating CD3⁺ and CD4⁺ T cells and among the highest frequency of infiltrating CD8⁺ T cells.

Further analyses of the paired pretreatment and posttreatment GBM revealed that the activated (PD-1⁺Ki-67⁺) tumor-infiltrating immune fraction increased 8.5-fold (from 5.2% to 44.2%) after neoadjuvant ICI therapy and was dominated by CD4⁺ T_{EM} cells (65.3%), followed by CD8⁺ (21.5%) and T_{reg} cells (12.4%; Fig. 2c,d). Activated granzyme B (GzmB)-expressing CD8⁺, CD4⁺ T_{EM} and CD4⁺ T_{reg} cells were also abundant (91%, 37% and 27%, respectively) in the posttreatment tumor (Fig. 2d). Transcriptome signatures indicative of immune cell activation, including IFN γ , chemokine, costimulatory and tumor inflammation gene sets were all elevated in the GBM tumor after ICI treatment (Fig. 2e). These changes in immune cell activity corresponded with complete occupancy of PD-1 by nivolumab on tumor-infiltrating CD8⁺ T, CD4⁺ T_{EM} and CD4⁺ T_{reg} cells in response to treatment (Fig. 2f). The expression of tumor major histocompatibility complex (MHC) classes I and II was examined after treatment; 83.8%, 75.3% and 72.7% of GFAP⁺/SOX2⁺ GBM cells expressed MHC class I, MHC class II or both MHC classes I and II, respectively (Fig. 3a). The immune checkpoints—LAG3, TIM3, CTLA-4, TIGIT and CD39—were all highly expressed in tumor-infiltrating T cells after treatment (Fig. 3b). Although there was insufficient pretreatment biopsy material to confirm checkpoint induction in response to ICI therapy in infiltrating immune cells, checkpoint expression was potentially induced from before to after neoadjuvant therapy in peripheral blood cell subsets (Fig. 4a,b).

The number of productive T cell receptor (TCR) β and TCR γ clonotypes and the Shannon diversity index of TCR β and TCR γ increased in the posttreatment tumor sample compared with the pretreatment specimen (Fig. 5a). Increased TCR diversity was associated with increased Shannon equitability (that is, similarity of clone frequency; Fig. 5a), confirming a more diverse TCR repertoire with reduced TCR clone dominance after neoadjuvant ICI therapy (Fig. 5b). TCR clone

Fig. 2 | Evaluation of immune cells in the GBM tumor before (day -4) and after (day +13) neoadjuvant ICI treatment. a, Representative region of whole-slide hematoxylin and eosin (H&E) and IHC images of paired pretreatment and posttreatment GBM specimens for CD3⁺, CD8⁺ and CD4⁺ T cells. Representative images were taken from areas of increased tumor cellularity. **b**, Representative region of whole-slide high-plex immunofluorescence images and cellular neighborhood enrichment analysis showing the co-occurrence of specific immune cells (CD8⁺ T and CD4⁺ T cells, dendritic cells (DCs), macrophages and glia) with tumor cells in the paired pretreatment and posttreatment GBM specimens. One slide was prepared and representative images were taken from areas of increased tumor cellularity. **c**, The tumor-infiltrating CD45⁺ (immune) fraction was analyzed for T cell content (CD3⁺), T cell subsets (CD8⁺, CD4⁺FOXP3⁻ T_{EM} and CD4⁺FOXP3⁺ T_{reg} cells) and activation markers (PD-1⁺Ki-67⁺). PD-1

expression on T cells was detected with anti-PD-1-Brilliant Violet 421 (BV421) in the pretreatment tumor or anti-IgG4-PE (detects nivolumab bound to PD-1) in the posttreatment tumor. **d**, The fraction of activated and proliferating T cell subsets, along with their GzmB expression, were evaluated in the posttreatment GBM. There was insufficient material available for analysis of the T cell subsets in the pretreatment biopsy specimen. **e**, Heatmap showing the immune activation transcriptome gene set³⁶ scores (derived from the singscore method³⁷) in the pretreatment and posttreatment tumor specimens (RNA was analyzed in triplet for each tumor specimen using the NanoString PanCancer IO360 Panel). **f**, The posttreatment tumor was analyzed for drug/nivolumab occupancy of PD-1 sites (nivolumab detection, staining with anti-IgG4-PE) and residual unoccupied PD-1 sites (PD-1 detection, staining with anti-PD-1 (CD279)-BV421). Scale bars = 100 μ m.



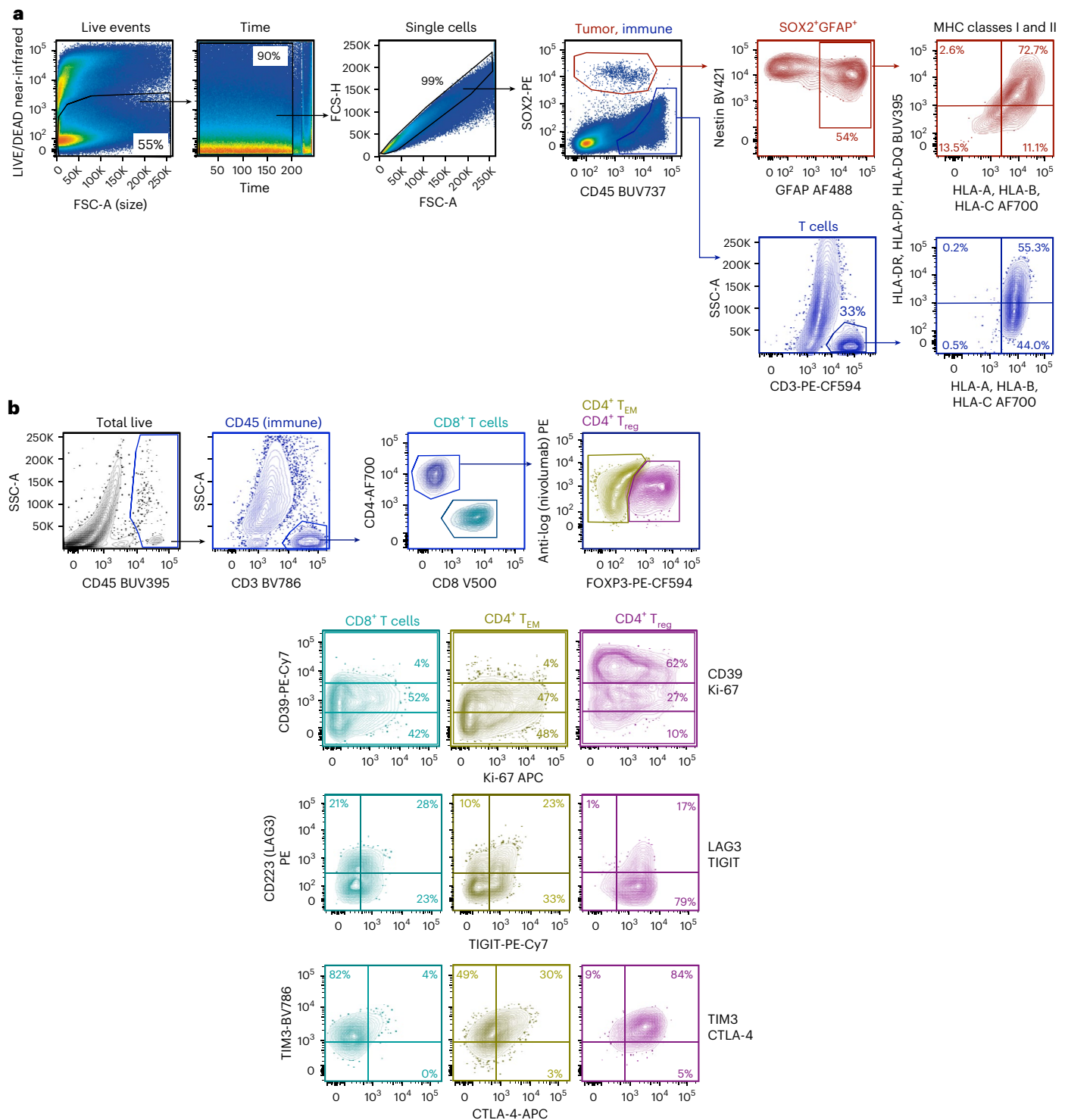


Fig. 3 | Flow cytometry tumor gating strategy and immune checkpoint analysis. **a**, General gating strategy for tumor dissociates. Left to right, a viability gate to exclude dead cells, a time gate to exclude electronic noise, a singlet gate to exclude doublets and tumor and immune fraction gates to define the cells of interest. Tumor cells (SOX2⁺) were further gated for the GFAP⁺ fraction and analyzed for MHC class I (HLA-A, HLA-B, HLA-C) and MHC class II (HLA-DR, HLA-DP, HLA-DQ) expression. The numbers indicate the percentage of cells

in the respective gates. T cell analysis is shown for comparison. **b**, The tumor-infiltrating CD45⁺ (immune) fraction was analyzed for T cell content (CD3⁺), T cell subsets (CD8⁺ T, CD4⁺FOXP3⁺ T_{EM} and CD4⁺FOXP3⁺ T_{reg} cells), and immune checkpoints (CD39, LAG3, TIGIT, TIM3 and CTLA-4). The numbers indicate the percentage of cells in the respective gates. BUUV, brilliant ultra-violet; FSC, forward scatter; FSC-A, forward scatter area; FSC-H, forward scatter height; SSC, side scatter; SSC-A, side scatter area.

sharing analysis confirmed that 63.65% of TCR β clones were uniquely identified in the tumor after treatment, whereas 28.21% of TCR β clones infiltrating the tumor after ICI therapy were also detected in the circulation (Fig. 5c,d). Importantly, TCR β clones shared between the

pretreatment, posttreatment and peripheral blood mononuclear cell (PBMC) samples were the most expanded clones (that is, TCR clones with more than 1% of the sample total TCR reads; Fig. 5e). These data suggest early clonal expansion of preexisting clonotypes.

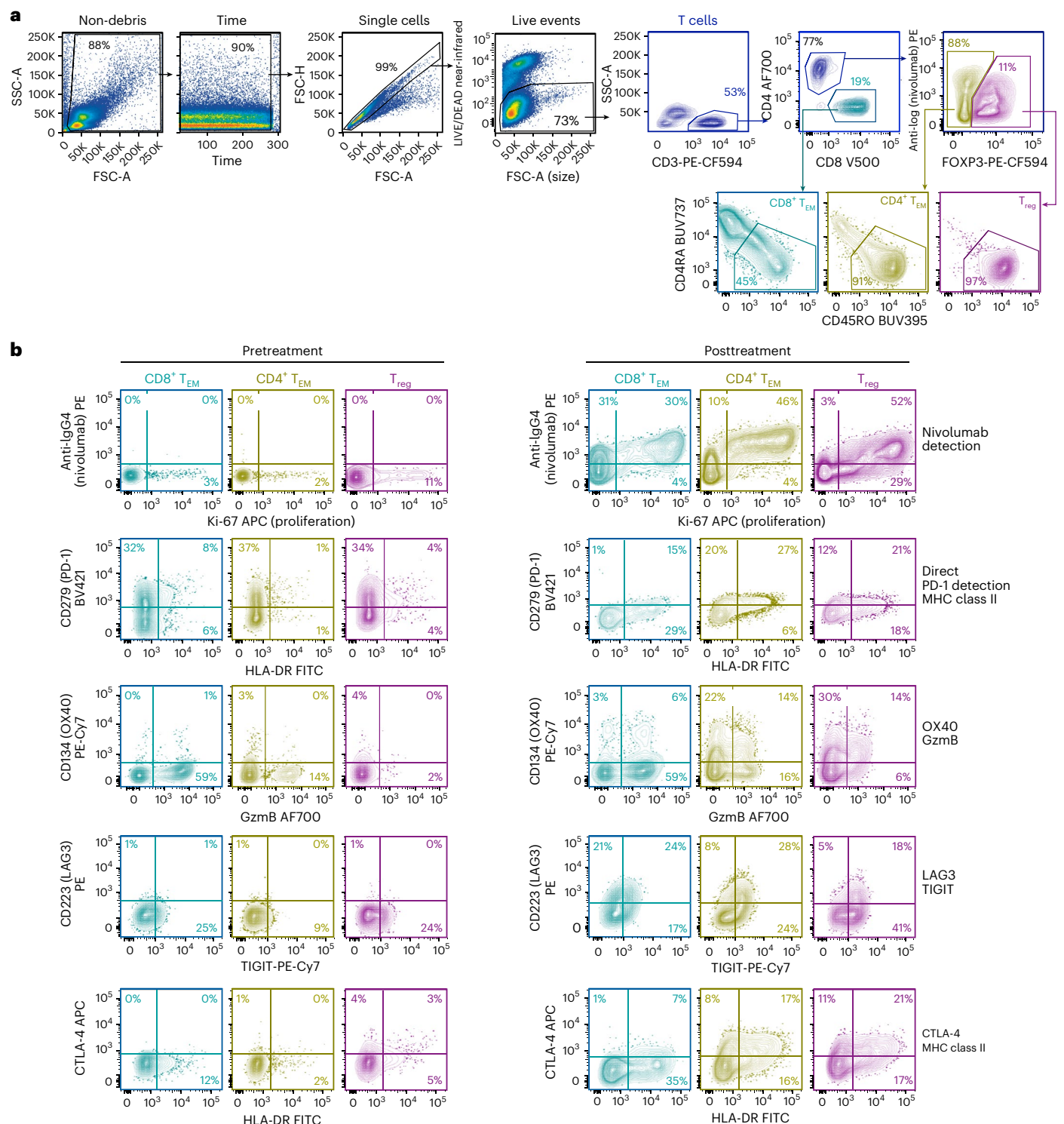


Fig. 4 | Evaluation of circulating T cells before and after neoadjuvant ICI treatment. a, General gating strategy for PBMC samples. Left to right, a debris exclusion gate, a time gate to exclude electronic noise, a singlet gate to exclude doublets and a viability gate to exclude dead cells. T cells (CD3⁺ SSC-A-low) were gated for CD45RA⁺ CD45RO⁺ effector and memory subsets: CD8⁺ T_{EM} (CD3⁺ CD8⁺ CD45RA⁺ CD45RO⁺), CD4⁺ T_{EM} (CD3⁺ CD4⁺ FOXP3⁺ CD45RA⁺ CD45RO⁺) and T_{reg} (CD3⁺ CD4⁺ FOXP3⁺ CD45RA⁺ CD45RO⁺) cells. **b**, CD8⁺ T_{EM}, CD4⁺ T_{EM} and T_{reg}

subsets in the pretreatment (day -4, left) and posttreatment (day +12, right) samples were analyzed for (top to bottom): T cell-bound nivolumab (detected with anti-IgG4-PE), residual unoccupied PD-1 (direct PD-1 detection with anti-PD-1 (CD279) BV421), activation markers (MHC class II, OX40) and GzmB. Immune checkpoint (LAG3, CTLA-4, TIGIT) expression analysis was performed on pretreatment (day -9) samples. The numbers indicate the percentage of cells in the respective gates.

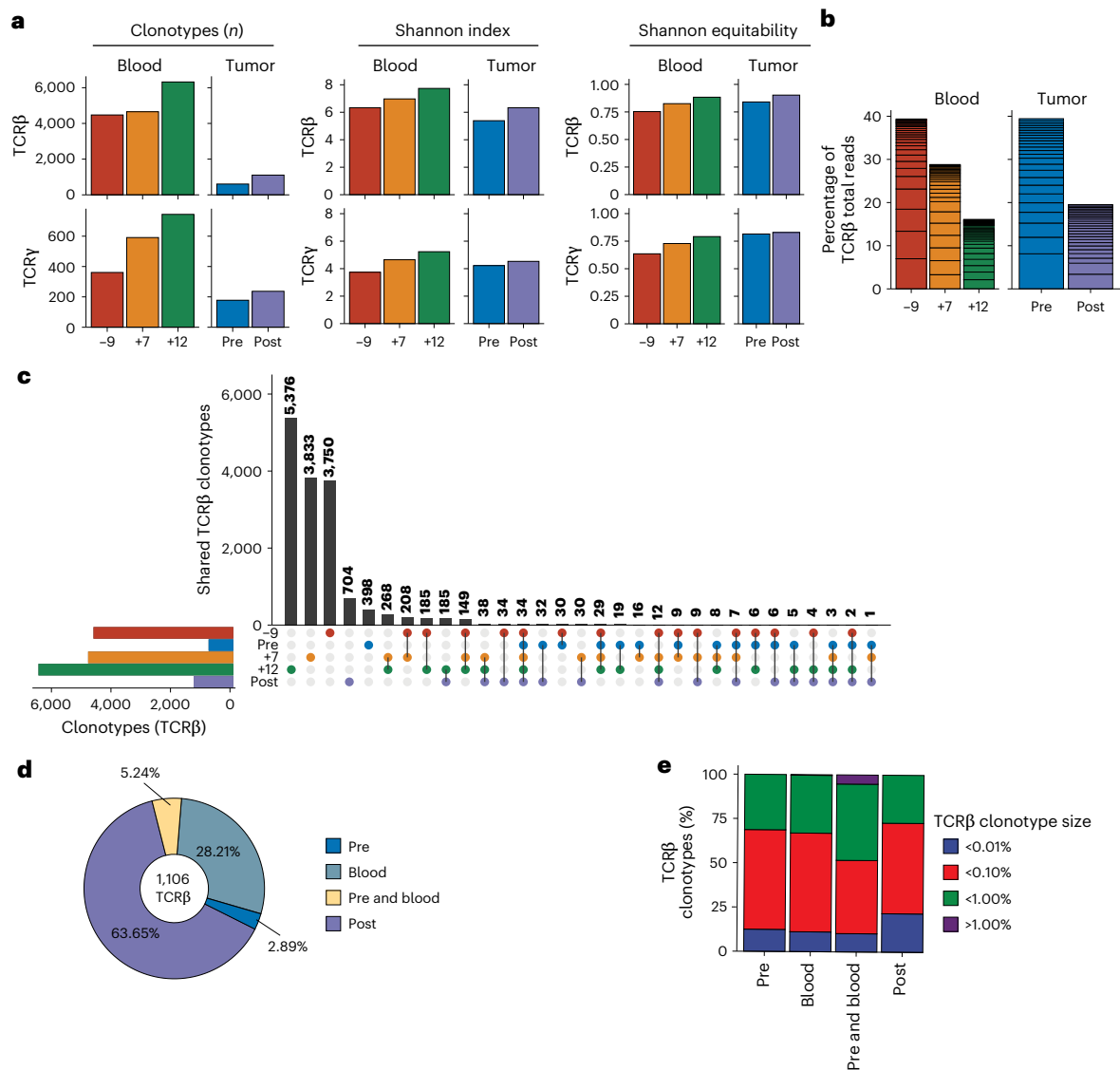


Fig. 5 | Neoadjuvant ICI-induced TCR repertoire and immune cell changes.

a, TCR β and TCR γ clone numbers, Shannon diversity index and Shannon equitability index scores (measurement of the similarity of clone sizes) increased after neoadjuvant ICIs in the tumor (pretreatment (day -4) and posttreatment (day +13)) and blood specimens (pretreatment (day -9) and posttreatment (days +7 and +12)). **b**, The TCR clone size (clonotype total reads expressed as a percentage of total productive reads) of the 25 largest TCR clonotypes in each sample. The largest clones are at the bottom of each column. **c**, Upset plot of the shared TCR β clonotypes across tumor (before and after) and blood specimens (day -9, day +7, day +12). The vertical bars indicate the number of clonotypes; the sample distribution patterns are indicated below the chart and are represented by filled points linked by the lines. A filled circle indicates that clones were detected in the corresponding samples; a gray circle indicates that TCR clones were not detected. The first five vertical bars show clonotypes unique

to each of the specimens. The horizontal bars (lower left) show the number of TCR β clones in each sample. **d**, Tracking the origin of clonotypes detected in the posttreatment tumor specimen. TCR β clonotypes were classified based on whether they were unique to the posttreatment sample (63.65% of clonotypes) or shared with any of the PBMC samples (blood), the pretreatment tumor sample or both the pretreatment tumor and blood samples. The number in the center indicates the number of productive TCR β clonotypes in the posttreatment tumor sample. **e**, Details of the size (clonotype total reads/sample total reads expressed as a percentage) of TCR β clonotypes identified in the posttreatment tumor according to their origin (that is, identified in PBMC sample (blood), the pretreatment tumor sample or both the pretreatment tumor and blood samples). Most expanded clones (accounting for more than 1% of the sample total reads) were shared with the pretreatment tumor and blood samples.

Dynamic changes in peripheral immune markers

Analysis of circulating TCR β and TCR γ in PBMC samples collected before treatment (day -9) and after treatment (days +7 and +12) confirmed an increasing number, diversity and equitability of TCR clones after neoadjuvant ICI therapy (Fig. 5a).

Peripheral blood cell subsets collected before treatment (day -9) and after treatment (day +12) with neoadjuvant ICI therapy were analyzed using flow cytometry. The posttreatment sample contained substantially higher percentages of proliferating effector and

memory (CD45+RA⁻RO⁺) CD8⁺, CD4⁺ T_{EM} and CD4⁺ T_{reg} (Ki-67⁺ fraction 34%, 50% and 81%, respectively; up from 3%, 2% and 11% in the pretreatment blood samples; Fig. 4b) cell subsets. The activation markers OX40 and MHC class II, and the cytotoxic marker GzmB, were each induced in circulating CD8⁺, CD4⁺ and T_{reg} subsets after neoadjuvant ICI therapy; PD-1 occupancy with nivolumab was also confirmed in these circulating T cells (Fig. 4b).

The Olink proximity extension assay quantified 725 immunology-related proteins in serum samples collected before (day -4)

and after (days +7 and +12) treatment with neoadjuvant ICI therapy. Most proteins (681 of 725; 94%) showed minimal changes in response to immunotherapy (log₂ fold change after treatment relative to before treatment, between -1 and +1). A distinct subset (44; 6%) proteins showed an increase or decrease of greater than twofold at days +7 and +12, compared with pretreatment protein levels (Extended Data Table 4). These proteins were associated with T cell activation and cytokine and interleukin (IL) signaling; they included the drug targets LAG3 and PDCD1, several ILs (IL5, IL6, IL10, IL12), the C-X-C motif chemokine ligands CXCL9 and CXCL10, and IFN γ .

Discussion

A single dose of neoadjuvant nivolumab, ipilimumab and relatlimab increased the diversity, abundance and activation of TILs in the post-treatment tumor compared with the baseline tumor in newly diagnosed *MGMT* promoter unmethylated GBM. In other settings, activation and expansion of TILs and peripheral T cells have been associated with an ICI response^{21–23}. While we observed features indicative of an ICI response, we cannot conclude that they predict clinical benefit for this patient. The binding of nivolumab to TILs confirms that intravenously administered ICIs can access the parenchyma of a primary brain tumor, whether via direct penetration or T cell-bound trafficking. Seventeen months after neoadjuvant combined (triplet) ICI, a maximal safe resection, adjuvant immunotherapies and a standard course of adjuvant radiotherapy, the patient has no definitive evidence of recurrence, which exceeds the median prognosis for this GBM when treated with chemoradiotherapy^{2,6}.

Our case highlights an opportunity to reexamine ICI for GBM with careful, data-driven and clinically informed optimization of neoadjuvant combination ICI in newly diagnosed GBM, without iatrogenic immunosuppression^{24–27}. Our concern is that the negative ICI studies in GBM, using adjuvant single-agent ICI in pretreated patients with recurrent disease, may have missed a critical early ‘window of opportunity’^{26,27} where ICI is ideally positioned to achieve a potentially curative response. Single-agent anti-PD-1 was not effective in patients with recurrent GBM who received prior chemotherapy and corticosteroids (~40% of patients at baseline were on prednisone at doses <10 mg, probably reduced for ‘trial eligibility’ in CheckMate 143) (refs. 12,28). Likewise, concurrent anti-PD-1 and radiotherapy did not improve the outcomes of newly diagnosed patients with GBM with unmethylated *MGMT* promoter, where nearly 30% of patients were receiving corticosteroids at baseline⁶. This scenario mirrors that of patients with melanoma brain metastasis, where those requiring corticosteroids for symptom management have a poorer response to ICIs than those not requiring steroids^{18,29}. Importantly, single-agent anti-PD-1 has demonstrated activity in isolated cases with GBM associated with germline mismatch repair deficiency^{30,31} and in newly diagnosed patients with *MGMT* methylated GBM treated in the neoadjuvant setting¹².

While single-agent anti-PD-1 shows limited benefit in most patient cohorts with GBM, combination ICIs target multiple independent steps in the cancer–immunity cycle; when dosed optimally, they improved patient outcomes compared with anti-PD-1 alone in cancers such as melanoma^{4,32,33}. A small feasibility study ($n = 15$, with nine patients unmethylated) reported a median OS of 19.3 months in newly diagnosed GBM treated with first-line adjuvant anti-PD-1 plus anti-CTLA-4, followed by standard radiotherapy³⁴. One important barrier to investigating combination ICI is the induction of immune-related adverse events, which may affect quality of life, require immunosuppression that counteracts the activity of ICI or result in early cessation of ICI treatment. In our case study, combined (triplet) ICI was continued by personalizing the therapy to immune-related toxicity (delaying cycles and reducing combinations as necessary). Another perceived barrier to the use of combination ICI in brain tumors is the risk of cerebral edema; however, this was not observed in this case nor in patients with melanoma with active brain metastases who had no prior radiotherapy¹⁸. The

perceived risk of using ICIs in GBM may be because of the concern of exacerbating radiotherapy-induced inflammation³⁵, especially given the doses and volumes of radiotherapy typically used in this tumor.

There are limitations to this research, namely, that the clinical outcomes and biospecimens were derived from a single patient and technical replication was often not feasible because of the limited amount of sample. The generalizability of these findings may also be limited by the favorable early disease course, including a rapid interval between presentation and diagnosis, no tumor growth between the diagnostic and preoperative scans, good Eastern Cooperative Oncology Group Performance Status and limited tumor-associated edema (although there were some key poor prognostic factors, including an unmethylated *MGMT* promoter and incomplete resection because of the tumor’s proximity to eloquent brain regions). If neoadjuvant ICI were trialed in newly diagnosed patients with GBM, the regimen would need to be rationally adapted to individual tumor and clinical factors.

This case study suggests that neoadjuvant combination ICI can promote the infiltration, activation and expansion of tumor-specific T cells in newly diagnosed GBM. A regimen of upfront combination ICIs in newly diagnosed GBM is worthy of more thorough investigation before these agents can be excluded from the GBM treatment algorithm; a clinical trial, GIANT (trial registration no. [NCT06816927](https://doi.org/10.1038/s41591-025-03512-1)), is planned.

Online content

Any methods, additional references, Nature Portfolio reporting summaries, source data, extended data, supplementary information, acknowledgements, peer review information; details of author contributions and competing interests; and statements of data and code availability are available at <https://doi.org/10.1038/s41591-025-03512-1>.

References

- Louis, D. N. et al. The 2021 WHO Classification of Tumors of the Central Nervous System: a summary. *Neuro Oncol.* **23**, 1231–1251 (2021).
- Stupp, R. et al. Radiotherapy plus concomitant and adjuvant temozolomide for glioblastoma. *N. Engl. J. Med.* **352**, 987–996 (2005).
- Ostrom, Q. T. et al. National-level overall survival patterns for molecularly-defined diffuse glioma types in the United States. *Neuro Oncol.* **25**, 799–807 (2023).
- Wolchok, J. D. et al. Final, 10-year outcomes with nivolumab plus ipilimumab in advanced melanoma. *N. Engl. J. Med.* **392**, 11–22 (2025).
- Sim, H.-W. et al. NUTMEG: a randomized phase II study of nivolumab and temozolomide versus temozolomide alone in newly diagnosed older patients with glioblastoma. *Neurooncol. Adv.* **5**, vdad124 (2023).
- Omuro, A. et al. Radiotherapy combined with nivolumab or temozolomide for newly diagnosed glioblastoma with unmethylated *MGMT* promoter: an international randomized phase III trial. *Neuro Oncol.* **25**, 123–134 (2023).
- Lim, M. et al. Phase III trial of chemoradiotherapy with temozolomide plus nivolumab or placebo for newly diagnosed glioblastoma with methylated *MGMT* promoter. *Neuro Oncol.* **24**, 1935–1949 (2022).
- Sharma, P., Aaroe, A., Liang, J. & Puduvali, V. K. Tumor microenvironment in glioblastoma: current and emerging concepts. *Neurooncol. Adv.* **5**, vdad009 (2023).
- Pombo Antunes, A. R. et al. Understanding the glioblastoma immune microenvironment as basis for the development of new immunotherapeutic strategies. *eLife* **9**, 52176 (2020).
- Lee, A. H. et al. Neoadjuvant PD-1 blockade induces T cell and cDC1 activation but fails to overcome the immunosuppressive tumor associated macrophages in recurrent glioblastoma. *Nat. Commun.* **12**, 6938 (2021).

11. Cloughesy, T. F. et al. Neoadjuvant anti-PD-1 immunotherapy promotes a survival benefit with intratumoral and systemic immune responses in recurrent glioblastoma. *Nat. Med.* **25**, 477–486 (2019).
12. Schalper, K. A. et al. Neoadjuvant nivolumab modifies the tumor immune microenvironment in resectable glioblastoma. *Nat. Med.* **25**, 470–476 (2019).
13. de Groot, J. et al. Window-of-opportunity clinical trial of pembrolizumab in patients with recurrent glioblastoma reveals predominance of immune-suppressive macrophages. *Neuro Oncol.* **22**, 539–549 (2020).
14. Dobersalske, C. et al. Cranioencephalic functional lymphoid units in glioblastoma. *Nat. Med.* **30**, 2947–2956 (2024).
15. Ascierto, P. A. et al. Efficacy and safety of triplet nivolumab, relatlimab, and ipilimumab (NIVO + RELA + IPI) in advanced melanoma: results from RELATIVITY-048. *J. Clin. Oncol.* **42**, 9504 (2024).
16. Gide, T. N. et al. Distinct immune cell populations define response to anti-PD-1 monotherapy and anti-PD-1/anti-CTLA-4 combined therapy. *Cancer Cell* **35**, 238–255 (2019).
17. Rozeman, E. A. et al. Survival and biomarker analyses from the OpACIN-neo and OpACIN neoadjuvant immunotherapy trials in stage III melanoma. *Nat. Med.* **27**, 256–263 (2021).
18. Long, G. V. et al. Ipilimumab plus nivolumab versus nivolumab alone in patients with melanoma brain metastases (ABC): 7-year follow-up of a multicentre, open-label, randomised phase 2 study. *Lancet Oncol.* [https://doi.org/10.1016/S1470-2045\(24\)00735-6](https://doi.org/10.1016/S1470-2045(24)00735-6) (2025).
19. Pires da Silva, I. et al. Ipilimumab alone or ipilimumab plus anti-PD-1 therapy in patients with metastatic melanoma resistant to anti-PD-(L)1 monotherapy: a multicentre, retrospective, cohort study. *Lancet Oncol.* **22**, 836–847 (2021).
20. Musca, B. et al. The immune cell landscape of glioblastoma patients highlights a myeloid-enriched and immune suppressed microenvironment compared to metastatic brain tumors. *Front. Immunol.* **14**, 1236824 (2023).
21. Stein, J. E. et al. Pan-tumor pathologic scoring of response to PD-(L)1 blockade. *Clin. Cancer Res.* **26**, 545–551 (2020).
22. Stein, J. E. et al. Major pathologic response on biopsy (MPRbx) in patients with advanced melanoma treated with anti-PD-1: evidence for an early, on-therapy biomarker of response. *Ann. Oncol.* **30**, 589–596 (2019).
23. Cottrell, T. R. et al. Pathologic features of response to neoadjuvant anti-PD-1 in resected non-small-cell lung carcinoma: a proposal for quantitative immune-related pathologic response criteria (irPRC). *Ann. Oncol.* **29**, 1853–1860 (2018).
24. Menzies, A. M. et al. Pathological response and survival with neoadjuvant therapy in melanoma: a pooled analysis from the International Neoadjuvant Melanoma Consortium (INMC). *Nat. Med.* **27**, 301–309 (2021).
25. Patel, S. P. et al. Neoadjuvant-adjuvant or adjuvant-only pembrolizumab in advanced melanoma. *N. Engl. J. Med.* **388**, 813–823 (2023).
26. Singh, K. et al. Correcting the drug development paradigm for glioblastoma requires serial tissue sampling. *Nat. Med.* **29**, 2402–2405 (2023).
27. Hotchkiss, K. M. et al. A brave new framework for glioma drug development. *Lancet Oncol.* **25**, e512–e519 (2024).
28. Reardon, D. A. et al. Effect of nivolumab vs bevacizumab in patients with recurrent glioblastoma: the CheckMate 143 phase 3 randomized clinical trial. *JAMA Oncol.* **6**, 1003–1010 (2020).
29. Tawbi, H. A. et al. Long-term outcomes of patients with active melanoma brain metastases treated with combination nivolumab plus ipilimumab (CheckMate 204): final results of an open-label, multicentre, phase 2 study. *Lancet Oncol.* **22**, 1692–1704 (2021).
30. Johanns, T. M. et al. Immunogenomics of hypermutated glioblastoma: a patient with germline *POLE* deficiency treated with checkpoint blockade immunotherapy. *Cancer Discov.* **6**, 1230–1236 (2016).
31. Bouffet, E. et al. Immune checkpoint inhibition for hypermutant glioblastoma multiforme resulting from germline biallelic mismatch repair deficiency. *J. Clin. Oncol.* **34**, 2206–2211 (2016).
32. Long, G. V. et al. Overall survival and response with nivolumab and relatlimab in advanced melanoma. *NEJM Evid.* **2**, EVIDoA2200239 (2023).
33. Tawbi, H. A. et al. Relatlimab and nivolumab versus nivolumab in untreated advanced melanoma. *N. Engl. J. Med.* **386**, 24–34 (2022).
34. Kesari, S. et al. Prospective phase I study of checkpoint blockade for the treatment of patients with newly diagnosed high-grade glioma prior to radiochemotherapy: results of nivolumab plus ipilimumab treatment arm. *J. Clin. Oncol.* **41**, 2057 (2023).
35. Raimbault, A. et al. Radionecrosis of malignant glioma and cerebral metastasis: a diagnostic challenge in MRI. *Diagn. Interv. Imaging* **95**, 985–1000 (2014).
36. Mao, Y. et al. Cross-platform comparison of immune signatures in immunotherapy-treated patients with advanced melanoma using a rank-based scoring approach. *J. Transl. Med.* **21**, 257 (2023).
37. Foroutan, M. et al. Single sample scoring of molecular phenotypes. *BMC Bioinformatics* **19**, 404 (2018).

Publisher's note Springer Nature remains neutral with regard to jurisdictional claims in published maps and institutional affiliations.

Open Access This article is licensed under a Creative Commons Attribution 4.0 International License, which permits use, sharing, adaptation, distribution and reproduction in any medium or format, as long as you give appropriate credit to the original author(s) and the source, provide a link to the Creative Commons licence, and indicate if changes were made. The images or other third party material in this article are included in the article's Creative Commons licence, unless indicated otherwise in a credit line to the material. If material is not included in the article's Creative Commons licence and your intended use is not permitted by statutory regulation or exceeds the permitted use, you will need to obtain permission directly from the copyright holder. To view a copy of this licence, visit <http://creativecommons.org/licenses/by/4.0/>.

© The Author(s) 2025

Georgina V. Long ^{1,2,3,4,5}✉, Elena Shklovskaya ^{1,6}, Laveniya Satgunaseelan ^{2,7}, Yizhe Mao ^{1,2,3}, Inês Pires da Silva ^{1,2,3}, Kristen A. Perry ^{1,2,3}, Russell J. Diefenbach ^{1,6}, Tuba N. Gide ^{1,2,3}, Brindha Shivalingam ^{1,7,8}, Michael E. Buckland ^{2,7}, Maria Gonzalez ¹, Nicole Caixeiro ^{1,2,3}, Ismael A. Vergara ^{1,2,3}, Xinyu Bai ^{1,2,3}, Robert V. Rawson ^{1,7,9}, Edward Hsiao ^{1,5}, Umaimainthan Palendira ^{2,3}, Tri Giang Phan ^{2,10}, Alexander M. Menzies ^{1,2,4,5}, Matteo S. Carlino ^{1,2,11,12}, Camelia Quek ^{1,2,3}, Sean M. Grimmond ^{13,14}, Joseph H. A. Vissers ^{13,14}, Dannel Yeo ^{2,15}, John E. J. Rasko ^{2,7,15}, Mustafa Khasraw ¹⁶, Bart Neyns ¹⁷, David A. Reardon ¹⁸, David M. Ashley ¹⁶, Helen Wheeler ⁵, Michael Back ^{5,19}, Richard A. Scolyer ^{1,2,3,7,9}, James Drummond ^{5,20,21}, James S. Wilmott ^{1,2,3} & Helen Rizos ^{1,6}

¹Melanoma Institute Australia, University of Sydney, Sydney, New South Wales, Australia. ²Faculty of Medicine and Health, University of Sydney, Sydney, New South Wales, Australia. ³Charles Perkins Centre, University of Sydney, Camperdown, New South Wales, Australia. ⁴Mater Hospital, North Sydney, New South Wales, Australia. ⁵Royal North Shore Hospital, St Leonards, New South Wales, Australia. ⁶Macquarie University, Macquarie Park, New South Wales, Australia. ⁷Royal Prince Alfred Hospital, Camperdown, New South Wales, Australia. ⁸Chris O'Brien Lifehouse, Camperdown, New South Wales, Australia. ⁹NSW Health Pathology, Sydney, New South Wales, Australia. ¹⁰Garvan Institute of Medical Research, Darlinghurst, New South Wales, Australia. ¹¹Blacktown Hospital, Blacktown, New South Wales, Australia. ¹²Westmead Hospital, Westmead, New South Wales, Australia. ¹³Collaborative Centre for Genomic Cancer Medicine, University of Melbourne, Melbourne, Victoria, Australia. ¹⁴Department of Clinical Pathology, University of Melbourne, Melbourne, Victoria, Australia. ¹⁵Centenary Institute, Camperdown, New South Wales, Australia. ¹⁶Duke University, Durham, NC, USA. ¹⁷Universitair Ziekenhuis Brussel, Brussels, Belgium. ¹⁸Center for Neuro-Oncology, Dana-Farber Cancer Institute, Boston, MA, USA. ¹⁹Sydney Medical School, University of Sydney, Sydney, New South Wales, Australia. ²⁰North Shore Radiology & Nuclear Medicine, St Leonards, New South Wales, Australia. ²¹Brain Imaging Laboratory, The Brain Cancer Group, St Leonards, New South Wales, Australia. ✉e-mail: georgina.long@sydney.edu.au

Methods

Patient and ethics

This research included a single 56-year-old white patient of male sex and gender. It was conducted in accordance with the Declaration of Helsinki (version 2024) and CAse REports guidelines, and with written informed consent of the patient. All drug therapy used in this study was obtained from Bristol Myers Squibb and submitted to the Therapeutic Goods Administration, Australia (Special Access Scheme, Category A). There was no participant compensation.

Biospecimen samples were acquired with consent from the Sydney Brain Tumour Bank (no. 2019/ETH08929), the Melanoma Biospecimen Tissue Bank (no. HREC/11/RPAH/444) and the Macquarie University Cancer Biobank (no. HREC2793). Tumor sequencing was performed with consent from the Royal Melbourne Hospital Office for Research (no. HREC/61352/MH-2020 34).

Next-generation sequencing and transcriptome analysis

WGS was performed on patient-matched normal and tumor DNA on the Illumina NovaSeq 6000 platform using the Illumina TruSeq Nano DNA library preparation kit according to the manufacturer's instructions³⁸. WGS analysis was performed using the Advanced Genomics Collaboration (TAGC) Clinical Genomics Analysis Platform to perform genome alignment (hg38) and variant calling using DRAGEN v.3.9 (refs. 39,40), copy number variation using PURPLE v.2.51 (ref. 41) and structural rearrangement detection via the DRAGEN SV and breakpointinspector v.1.5 packages and prioritized using the simple_sv_annotation⁴². All workflows are written in the Common Workflow Language and are freely available under the MIT license in a version-controlled repository (<https://github.com/umccr/cwl-ica>).

Total RNA samples were used as input for the NanoString IO 360 Panel and run on the nCounter Max/Flex Prep Station and Digital Analyzer³⁶. Calculation of signature scores was performed using the singscore method from the raw read count table^{36,37}.

Flow cytometry analysis

Flow cytometry staining was performed on viable cryopreserved tumor or PBMC samples¹⁰. Samples were thawed and stained with fluorophore-conjugated antibodies against the following: CD45 (BUV737, clone HI30; 1/200 dilution, cat. no. 748719; research resource ID (RRID): AB_2873123); CD45RA (BUV737, clone HI10; 1/100 dilution, cat. no. 564442; RRID: AB_2738810); CD45RO (BUV395, clone UCHL1; 1/20 dilution, cat. no. 564291; RRID: AB_2744410); CD3 (PE-CF594, clone UCHT1; 1/100 dilution, cat. no. 562280; RRID: AB_11153674); CD3 (BV786, clone UCHT1; 1/100 dilution, cat. no. 565491; RRID: AB_2739260); HLA-DR, HLA-DP, HLA-DQ (BUV395, clone Tu39; 1/200 dilution, cat. no. 740302; RRID: AB_2740041); CD8 (V500, clone SK1; 1/100 dilution, cat. no. 561617; RRID: AB_10896281); CD134 (OX40, PE-Cy7, clone Ber-ACT35; 1/20 dilution, cat. no. 563663; RRID: AB_2738358) (all were obtained from BD Biosciences); HLA-A, HLA-B, HLA-C (AF700, clone W6/32; 1/80 dilution, cat. no. 311438; RRID: AB_2566306); CD4 (AF700, clone A161A1; 1/40 dilution, cat. no. 357418; RRID: AB_2616933); HLA-DR (FITC, clone L243; 1/100 dilution, cat. no. 307604; RRID: AB_314682) (all from BioLegend); and CD223 (LAG3, PE, clone REA351; 1/11 dilution, cat. no. 130-105-452, Miltenyi Biotech; RRID: AB_2656407). Nonspecific staining was blocked with Fc block (clone Fc1, 1/200 dilution, cat. no. 564220, BD Biosciences; RRID: AB_2728082). For the detection of T cell-bound nivolumab, cells were incubated with human IgG4Fc (PE, clone HP6025; 1/100 dilution, cat. no. 9200-09, Southern Biotech; RRID: AB_2796693). For direct PD-1 detection, cells were stained with CD279 (PD-1, BV421, clone EH12.1; 1/50 dilution; cat. no. 562516, BD Biosciences; RRID: AB_11153482). Cell viability was determined by staining cells with LIVE/DEAD near-infrared fixable dye (cat. no. L34976, Thermo Fisher Scientific).

After cell surface staining, cells were fixed and permeabilized using the eBioscience Transcription Factor Buffer Kit (cat. no. 00-5523-00,

Thermo Fisher Scientific) and stained with the following antibodies plus Fc block in permeabilization buffer: FOXP3 (PE-CF594, clone 236A/E7; 1/20 dilution, cat. no. 563955; RRID: AB_2738507); GFAP (AF488, clone 1B4; 1/20 dilution, cat. no. 560297; RRID: AB_1645350); GzmB (AF700, clone GB1; 1/100 dilution, cat. no. 560213; RRID: AB_1645453); SOX2 (PE, clone O30-678; 1/100 dilution, cat. no. 562195; RRID: AB_10895118) (all from BD Biosciences); CD152 (CTLA-4, APC, clone 14D3; 1/20 dilution, cat. no. 17-1529-42; RRID: AB_2688162); Ki-67 (APC, clone 20Raj1; 1/150 dilution, cat. no. 17-5699-42; RRID: AB_2573218) (both from Thermo Fisher Scientific). Samples were washed extensively and immediately acquired on a BD LSRFortessa X20 flow cytometer (BD Biosciences). Samples were analyzed with the FlowJo software v.10.8 (BD Biosciences).

PhenoCycler–Fusion tissue imaging and analysis

Antibodies targeting tumor and non-tumor cells in the TME were conjugated to short DNA oligonucleotides and titrated according to the manufacturer's instructions (Akoya Biosciences)⁴³. Antigens shown in this study include the following: CD14 (AKYP0079, 1/200 dilution, Akoya Biosciences), CD11c (AKYP0051, 1/400 dilution, Akoya Biosciences), CD141 (AKP0124, 1/200 dilution, Akoya Biosciences), CD3 (AKYP0062, 1/200 dilution, Akoya Biosciences), CD8 (AKYP0028, 1/200 dilution, Akoya Biosciences), CD4 (AKYP0048, 1/200 dilution, Akoya Biosciences), GzmB (AKYP0086, 1/100 dilution, Akoya Biosciences), FOXP3 (AKYP0086, 1/100 dilution, Akoya Biosciences) and S100B (1/200 dilution, cat. no. 42397, Cell Signaling Technology). Initial T cell quantification was performed using the HALO AI v.3.6 image analysis platform with default artificial intelligence-based cell sequencing and manual gating of T cell phenotypes. Subsequent broad immunophenotyping was performed with cell segmentation in StarDist using the DAPI channel (cytoplasm segmentation was estimated using a morphological dilation of 5 μ m); cell phenotyping for CD4⁺ and CD8⁺ T cells was performed using the machine learning classifier in QuPath v.0.4.4 (ref. 44). Cell neighborhood enrichment analysis was performed using a graph-based connectivity algorithm with the squidpy Python package⁴⁵. Cell proximity in spatial neighborhoods was quantified with a permutation-based test (1,000 default) by comparing the spatial location of cell types and their relative distances.

TCR pan-clonality assay

DNA target amplification (200 ng genomic DNA input), partial digestion, barcoding of amplicons and purification were performed according to the manufacturer's protocol (Oncomine Human Immune Repertoire user guide for TCR pan-clonality assay, Thermo Fisher Scientific). The barcoding set consisted of the IonTorrent Dual Barcode Kit 1–96 (Thermo Fisher Scientific). Target amplification was for 31 cycles.

Purified libraries were quantified with quantitative PCR (qPCR) using an Ion Library TaqMan Quantitation Kit (Thermo Fisher Scientific) according to the Oncomine Human Immune Repertoire user guide. A 1/100 dilution of each sample library was analyzed in each case. qPCR was performed using a QuantStudio 7 Pro qPCR system (Thermo Fisher Scientific) in standard run mode (Oncomine Human Immune Repertoire user guide). Individual barcoded libraries were diluted to a final concentration of 50 pM in nuclease-free water using Eppendorf DNA LoBind microcentrifuge tubes (Sigma-Aldrich). For each sequencing chip, equal volumes (5 μ l) of 12 diluted library samples were combined on ice. Subsequently, 25 μ l of the pooled libraries were used for template preparation and chip loading.

The sequencing workflow consisted of template preparation and sequencing chip loading on an Ion Chef instrument (Thermo Fisher Scientific), sequencing on an Ion GeneStudio S5 plus system (Thermo Fisher Scientific) followed by data analysis. Planned sequencing runs were based on the Oncomine TCR Pan-Clonality Assay using the Torrent

Suite software v.5.18.1. The kits used for each planned sequencing run were an Ion 550 Kit–Chef, Ion S5 Sequencing Kit and Ion 550 chip (Thermo Fisher Scientific). Sequencing data were automatically uploaded to the Ion reporter software v.5.18.4 for analysis using the Oncombine TCR Beta-SR and Gamma-SR–w1.4–DNA Single Sample workflow. Multi-sample analysis was based on join CDR3 nt.

Clonotypes were defined using V, J and CDR3 amino acid sequences from the TCR β and TCR γ clone summaries from Thermo Fisher Scientific Ion Torrent targeted next-generation sequencing assay. Nonproductive clonotypes, based on the ‘functionality’ field, were excluded from the analysis. The productive clonotype frequency was calculated based on the total number of reads for a clonotype divided by the total number of productive reads in the sample. Clonotype diversity Shannon entropy (H) was calculated based on the clonotype abundances in each sample using $H = -\sum p_i \times \ln(p_i)$, where p_i is the proportion of sequence i relative to the total N sequences⁴⁶. Maximum Shannon diversity was calculated as $\ln(\text{total clonotypes})$. The Shannon equitability or evenness was calculated as $H/(\text{max diversity})$.

Distribution of clonotypes in each sample

Clonotypes were ranked according to their frequency, from largest to smallest, using `min_rank` from the `dplyr` R package (<https://dplyr.tidyverse.org>)⁴⁷. The `min_rank` approach gives every tie the same (smallest) value. The cumulative frequency for the ranked clonotypes in each sample was calculated using the `cumsum` function from base R. Data analysis was performed in R v.4.3.0 (21 April 2023 release) using RStudio v.4.3.0 (<https://cran.r-project.org/bin/windows/base/old/4.3.0/>, ref. 48) with the following R packages: `tidyverse` v.2.0.0 (ref. 49); `ggpubr` (<https://cran.r-project.org/web/packages/ggpubr/index.html>); `ggsci` v.3.0.0 (<https://github.com/nanxstats/ggsci>); `lemon` v.0.4.9 (<https://github.com/stefanedwards/lemon>); and `UpSetR` v.1.4.0 (<https://CRAN.R-project.org/package=UpSetR>).

Proximity extension assay

Plasma samples collected before (day –4) and after treatment (days +7 and +12) were analyzed using the proximity extension assay at the Olink Proteomics facility, Uppsala, Sweden. In total, 725 immuno-oncology-related protein biomarkers (Olink Explore 384 Inflammation, Olink Explore 384 Oncology (www.olink.com)) were measured and reported as normalized protein expression values, which is an arbitrary unit on a log₂ scale, where a higher value corresponds to higher protein expression.

CTC analysis

A total of 7.5 ml whole-blood samples were processed using the AccuCyte–CyteFinder platform (RareCyte)⁵⁰. Nucleated blood cells were isolated using AccuCyte (RareCyte) and spread onto eight SuperFrost Plus slides (Thermo Fisher Scientific). Slides were immunofluorescently stained on the Autostainer Link 48 (Agilent Technologies) using the following: anti-GFAP (AF488; cat. no. 560297, Becton Dickinson), anti-EGFR (PE; cat. no. FAB9577P, R&D Systems), anti-CD45 (AF750; cat. no. NBP1-79127AF750, Novus Biologicals), anti-CD66b (AF750; cat. no. FAB42462, R&D Systems) antibodies and a nuclear DAPI dye (Thermo Fisher Scientific). Slides were then scanned on the CyteFinder HT (RareCyte) digital immunofluorescence microscope at $\times 10$ magnification, with the following exposure times: 0.05 s (DAPI); 0.01 s (GFAP); 0.1 s (EGFR); and 0.1 s (CD45/CD66b). Image files were analyzed using an automated software and presented to the reviewer for CTC confirmation (CyteMapper, RareCyte). A CTC was defined as positive for DAPI and GFAP, and negative for CD45/CD66b (mean fluorescence intensity cutoff = 15).

Reporting summary

Further information on research design is available in the Nature Portfolio Reporting Summary linked to this article.

Data availability

Requests for data access will be reviewed by the senior authors. Applicants can expect a response within 2 weeks of submission. Data will be provided under the following conditions: (1) the research must have received ethical approval from a recognized ethics review board; (2) the request must align with the scientific aims and goals of the dataset; (3) the requesting team must demonstrate the ability to handle the data securely and responsibly; (4) a formal data usage agreement must be signed, ensuring that the data will not be used for commercial purposes and will not be shared with unauthorized parties. Source data are provided with this paper.

References

- Mann, G. B. et al. Postoperative radiotherapy omission in selected patients with early breast cancer following preoperative breast MRI (PROSPECT): primary results of a prospective two-arm study. *Lancet* **403**, 261–270 (2024).
- Zhao, S., Agafonov, O., Azab, A., Stokowy, T. & Hovig, E. Accuracy and efficiency of germline variant calling pipelines for human genome data. *Sci. Rep.* **10**, 20222 (2020).
- Behera, S. et al. Comprehensive genome analysis and variant detection at scale using DRAGEN. *Nat. Biotechnol.* <https://doi.org/10.1038/s41587-024-02382-1> (2024).
- Priestley, P. et al. Pan-cancer whole-genome analyses of metastatic solid tumours. *Nature* **575**, 210–216 (2019).
- Ahdesmäki, M. J. et al. Prioritisation of structural variant calls in cancer genomes. *PeerJ* **5**, e3166 (2017).
- Black, S. et al. CODEX multiplexed tissue imaging with DNA-conjugated antibodies. *Nat. Protoc.* **16**, 3802–3835 (2021).
- Bankhead, P. et al. QuPath: open source software for digital pathology image analysis. *Sci. Rep.* **7**, 16878 (2017).
- Palla, G. et al. Squidpy: a scalable framework for spatial omics analysis. *Nat. Methods* **19**, 171–178 (2022).
- Shannon, C. E. A mathematical theory of communication. *Bell Syst. Tech. J.* **27**, 379–423 (1948).
- Wickham, H., François, R., Henry, L., Müller, K. & Vaughan, D. `dplyr`: a grammar of data manipulation. R package version 1.1.4 <https://dplyr.tidyverse.org> (2023).
- R Core Team. *R: A Language and Environment for Statistical Computing* (R Project for Statistical Computing, 2023).
- Wickham, H. et al. Welcome to the Tidyverse. *J. Open Source Software* **4**, 1686 (2019).
- Yeo, D. et al. Accurate isolation and detection of circulating tumor cells using enrichment-free multiparametric high resolution imaging. *Front. Oncol.* **13**, 1141228 (2023).

Acknowledgements

We thank A. Bastian for antibody optimization and blood sample processing for the CTC analysis, K. Jackson for her expertise with TCR analysis and B. Pedersen for expertise with the flow cytometry experiments. We thank K. Pham, O. Hofmann and the Collaborative Centre for Genomic Cancer Medicine for performing the WGS analysis and J. Checkley and the Macquarie University Cancer Biobank for providing the GBM tumor dissociates. WGS was performed as part of the COLUMN initiative. The authors received no specific funding for this work. Investigators were supported by Melanoma Institute Australia (C.Q.), National Health and Medical Research Council Investigator grants (to G.V.L., R.A.S., T.G.P., A.M.M. and J.S.W.), Cancer Institute NSW grants (no. 2020/ECF1153 to C.Q.; no. 2020/ECF1244 to T.N.G.; no. 2021/CBG0002 to D.Y.), NSW Health Early-Mid Career grants (to C.Q.), the University of Sydney Medical School Foundation (G.V.L.), the CLEARbridge Foundation (R.J.D.), N. and H. Moore (A.M.M.) and PhD scholarships from the University of Sydney and Melanoma Institute Australia (X.B.). We thank Bristol Myers Squibb for providing the study drugs nivolumab, relatlimab and ipilimumab. Bristol Myers

Squibb had no role in study design, data collection and analysis, decision to publish or preparation of the manuscript.

Author contributions

G.V.L. conceived and designed the study treatment and biospecimen collection, recruited the patient, coordinated the study treatment and designed and interpreted the scientific experiments and analyses. G.V.L. was responsible for the administration, clinical care and monitoring of the immunotherapy and vaccine treatment, and for monitoring the response. H.R. provided scientific oversight, designed the scientific experiments and analyses, generated the data and performed the data analysis and interpretation. E.S., Y.M., I.P.d.S., X.B., C.Q., I.A.V., T.G.P., T.N.G., D.Y., J.E.J.R., R.J.D., S.M.G., J.H.A.V., U.P. and J.S.W. designed the scientific experiments, generated the data and performed the data analysis. G.V.L., J.S.W. and H.R. provided project management and data storage and consolidation. B.S. performed all neurosurgical interventions and advised on timing of surgery. M.B. was responsible for the administration of radiotherapy and for monitoring the response. H.W. was responsible for the neuro-oncology clinical care and for monitoring the response. J.D. and E.H. reviewed and interpreted the radiology data. N.C. and M.G. coordinated and performed the biospecimen collection, processing and storage, and provided operational support. L.S. and M.E.B. performed the pathological processing and analysis. R.V.R. and R.A.S. reviewed the pathology specimens. I.P.d.S., A.M.M., M.S.C., B.N., D.A.R., D.M.A. and M.K. provided clinical support. K.A.P. performed the literature review, consolidated the data and aided in the interpretation of the results. G.V.L., H.R. and K.A.P. collaboratively wrote all the manuscript drafts. All authors reviewed the results and the manuscript and approved the final version.

Funding

Open access funding provided by the University of Sydney.

Competing interests

G.V.L. is consultant adviser for Agenus, Amgen, Array Biopharma, AstraZeneca, Bayer, BioNTech, Boehringer Ingelheim, Bristol Myers Squibb, Evaxion, Hexal AG (a Sandoz Company), Highlight Therapeutics, IOBiotech, Immunocore, Innovent Biologics USA, Merck Sharpe & Dohme, Novartis, PHMR Ltd, Pierre Fabre and Regeneron. R.V.R. has received an honorarium from Merck Sharpe & Dohme. M.S.C. has served on advisory boards or as a consultant for Amgen, Bristol Myers Squibb, Eisai, Ideaya, Merck Sharpe & Dohme, Nektar, Novartis, Oncosec, Pierre Fabre, Qbiotics, Regeneron, Roche, Merck KGaA and Sanofi, and received honoraria from Bristol Myers Squibb, Merck Sharpe & Dohme and Novartis. D.E.G. has served on advisory boards for Amgen and received honoraria from Bristol Myers Squibb and Merck Sharpe & Dohme. J.E.J.R. reports advisory roles for the Gene Technology Technical Advisory Committee, the Office of the Gene Technology Regulator, the Australian Government and the Human

Research Ethics Committee of Geneva. J.E.J.R. also reports honoraria, speaker fees or advisory roles for SPARK Therapeutics, Cynata and Pfizer; shares in Woke Pharmaceutical; is a nonexecutive director of Kennerton Capital; is a cofounder of AAVec Bio; and a consultant role for RareCyteand, with stocks in lieu. A.M.M. has served on advisory boards for Bristol Myers Squibb, Merck Sharpe & Dohme, Novartis, Roche, Pierre Fabre and Qbiotics. I.P.d.S. declares honoraria, speaker fees or advisory roles for Pierre Fabre, Merck Sharpe & Dohme, Roche, Novartis and Bristol Myers Squibb, and has served as consultant on advisory boards for Merck Sharpe & Dohme. D.A.R. has received honoraria for serving on advisory boards or as a consultant for Agenus, Avita Biomedical, Bayer, Blue Rock Therapeutics, Boston Biomedical, Boehringer Ingelheim, Bristol Myers Squibb, CeCava, Chimeric Therapeutics, Deciphera, Ellipses Pharma, EMD Serono, Genentech/Roche, Imvax, Inovio, Medicenna Biopharma, Merck Sharpe & Dohme, Merck KGaA, Monteris, Novartis, Oncorus, Oxigene, Regeneron and Taiho Oncology. He has stocks in AnHeart Therapeutics and Bionaut Labs. Laboratory research support for his work has been paid to the Dana-Farber Cancer Institute by Enterome, NeoTX Ltd (240K) and Ashvattha Therapeutics (119K). M.K. reports grants or contracts from Bristol Myers Squibb, AbbVie, BioNTech, CNS Pharmaceuticals, Daiichi Sankyo, Immorna Therapeutics, Immvira Therapeutics, JAX lab for genomic research and Personalis; he has received consulting fees from AnHeart Therapeutics, Berg Pharma, George Clinical, Manarini Stemline and Servier; he has received honoraria from GlaxoSmithKline; and is on a data safety monitoring board for BPGbio. R.A.S. has received fees for professional services from SkylineDx, IO Biotech, MetaOptima Technology, Roche, Evaxion, Provectus Biopharmaceuticals Australia, Qbiotics, Novartis, Merck Sharp & Dohme, NeraCare, Amgen, Bristol Myers Squibb, Myriad Genetics and GlaxoSmithKline. R.A.S. is both the subject and an author of this study. The other authors declare no competing interests.

Additional information

Extended data is available for this paper at

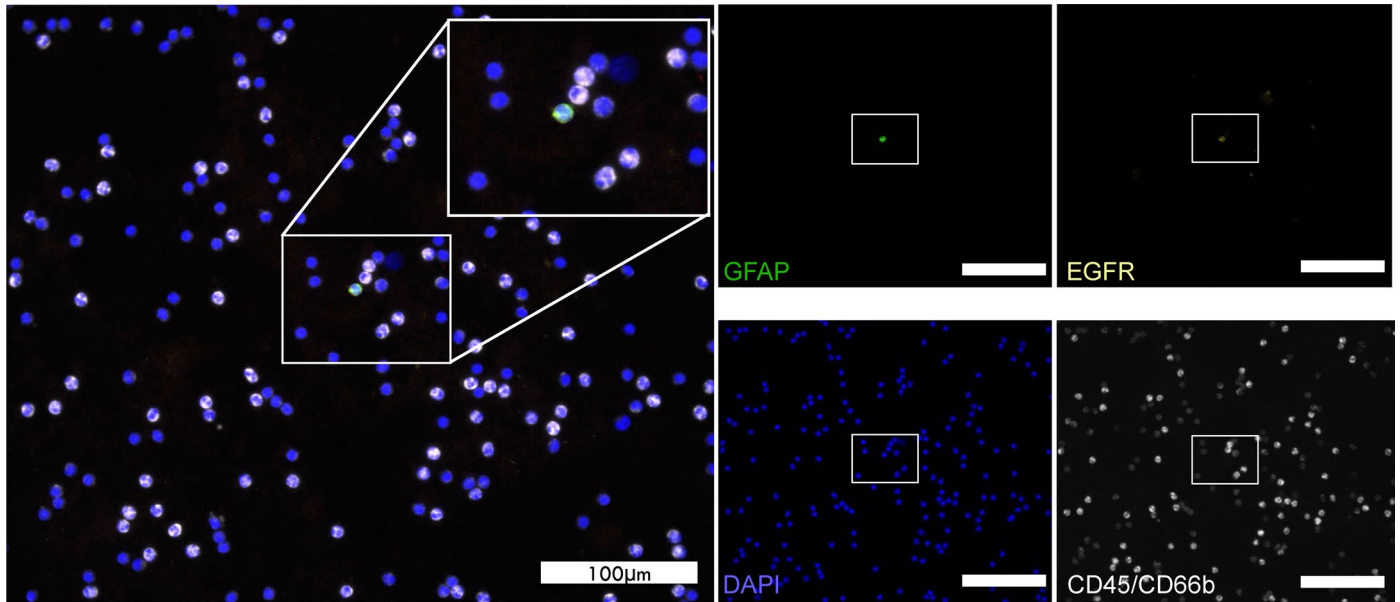
<https://doi.org/10.1038/s41591-025-03512-1>.

Supplementary information The online version contains supplementary material available at <https://doi.org/10.1038/s41591-025-03512-1>.

Correspondence and requests for materials should be addressed to Georgina V. Long.

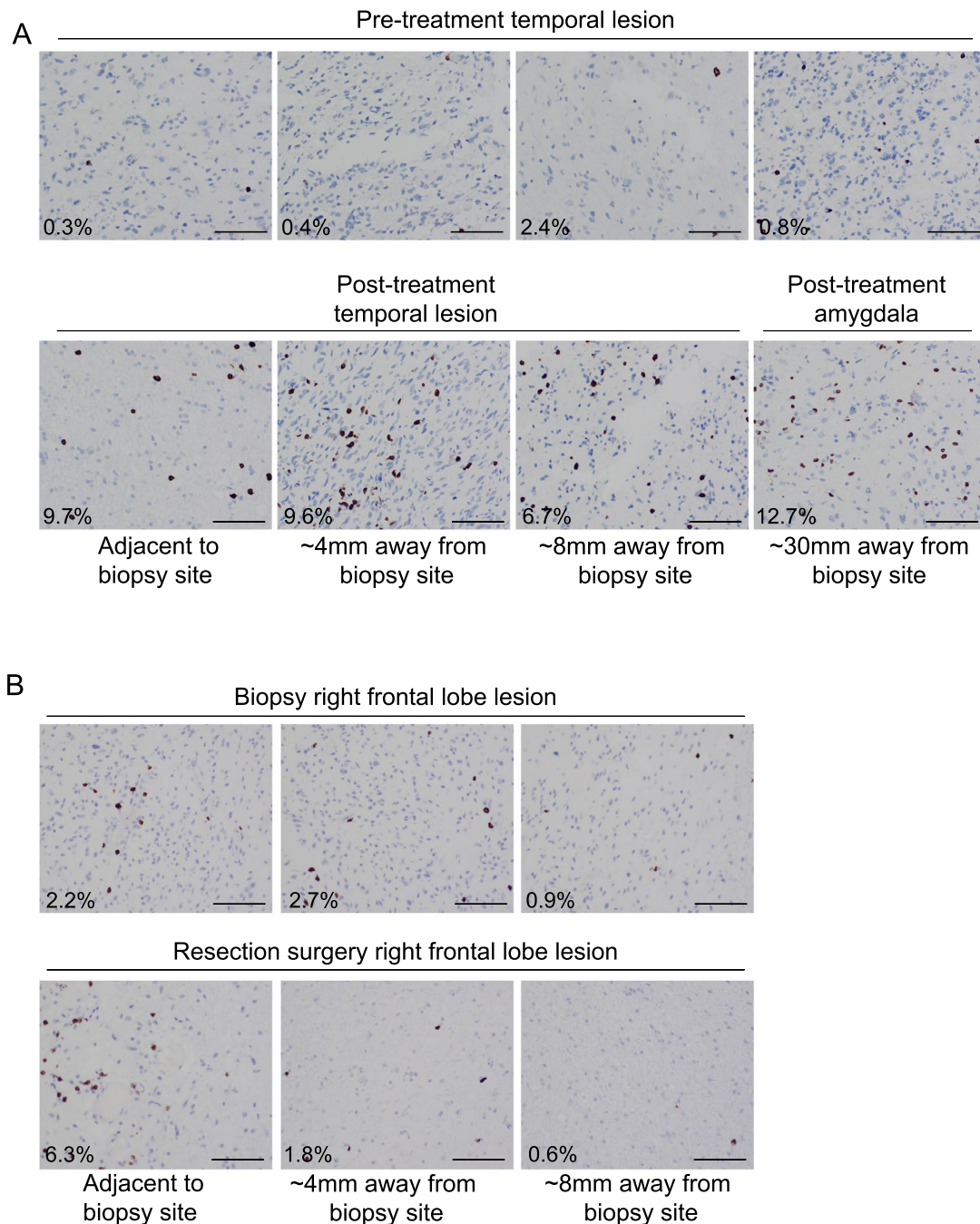
Peer review information *Nature Medicine* thanks the anonymous reviewers for their contribution to the peer review of this work. Primary Handling Editor: Ulrike Harjes, in collaboration with the *Nature Medicine* team.

Reprints and permissions information is available at www.nature.com/reprints.



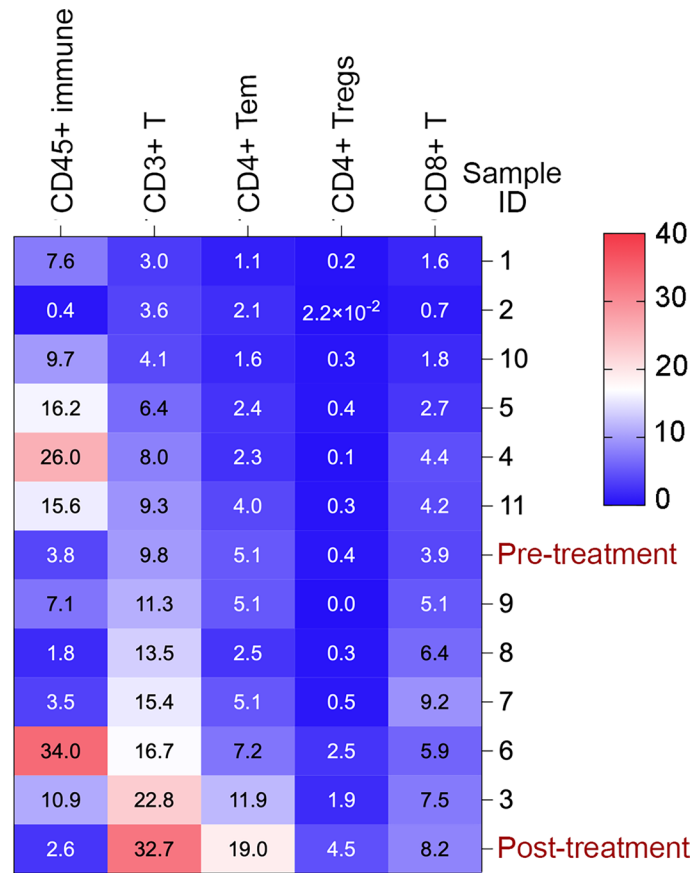
Extended Data Fig. 1 | Identification of circulating tumor cells. Representative region of whole-slide immunofluorescence showing circulating tumor cell (CTC, boxed) identified in a GBM patient. Cells were stained for GFAP (green), EGFR (yellow), CD45/CD66b (white) and nuclear DAPI (blue). Magnification, 40X. Sample collected pretreatment (day -9). 7.5 mL peripheral blood was processed

on the AccuCyte-CyteFinder platform (RareCyte). Nucleated blood cells were spread on 8 slides. Slides were stained using DAKO autostainer and the whole slide was imaged and analyzed by CyteMapper software for DAPI⁺ GFAP⁺ EGFR^{+/-} CD45/CD66b⁻ cells with user verification. Scale bars = 100 µm.



Extended Data Fig. 2 | Evaluation of CD3⁺ immune cells in longitudinal GBM biopsy and surgical specimens in A) the ICI-treated left temporal GBM and B) an untreated right frontal GBM. a) Representative region of whole-slide immunohistochemistry images of pretreatment (day -4) and posttreatment (day +13) GBM specimens for CD3⁺ T cells across left temporal and amygdala sections. Percentage CD3⁺ T cell content is shown and was quantitated from over 1,300 cells in each tissue specimen using QuPath. Representative regions were taken from areas of increased tumor cellularity. b) Representative region

of whole-slide immunohistochemistry images showing CD3⁺ T cell infiltration in biopsy and resection specimens from a 66-year-old male with right frontal lobe GBM. The patient underwent an initial diagnostic biopsy, followed by maximal tumor resection 14 days later. Percentage CD3⁺ T cell content is shown and was quantitated from over 1,200 cells in each tissue specimen using QuPath. Representative regions were taken from areas of increased tumor cellularity. Scale bars = 100 μ m.



Extended Data Fig. 3 | Frequency of lymphocyte subsets in primary GBM. Heat map showing frequency of lymphocyte subsets in primary GBM tumor dissociates (n = 13), including the pretreatment and posttreatment GBM tumor dissociates (highlighted in red). Samples are ranked according to CD3⁺ T cell

content. T cell subsets (CD3⁺ T cells, CD4⁺FOXP3⁺ regulatory T cells (Tregs), CD4⁺FOXP3⁻ effector memory T cells (Tem) and CD8⁺ T cells) are shown as percentage of total CD45⁺ cells. CD45⁺ lymphocytes are shown as percentage of viable cells.

Extended Data Table 1 | Neoadjuvant immune checkpoint inhibitor trials in glioblastoma

Trial	Pts, <i>n</i>		Design	Treatment		Outcomes		Tumor and peripheral immune features post-neoadjuvant
	Rec.	New		Neoadjuvant	Adjuvant	mOS, mo. (95% CI)	mPFS, mo. (95% CI)	
Cloughesy ¹¹	35	0	Two arm, randomized, neo+adj vs adj	1x pembro. 200 mg 14+5 days pre-surgery	Pembro. 200 mg Q3W	neo+adj: 13.7 (NR) adj: 7.5 (NR) HR 0.39 (0.17–0.94) <i>p</i> =0.04	neo+adj: 3.3 (NR) adj: 2.4 (NR) HR 0.43 (0.20–0.90) <i>p</i> =0.03	↑Intratumoral CD8+ T cell clones ↑T cell- and IFN γ -related transcripts ↑Intratumoral PD-L1 expression ↓Tumoral cell cycle transcripts ↓PD-1 on peripheral T cells ↓Peripheral monocytes
Schalper ¹²	27	3	Single arm, neo+adj	1x nivo. 3 mg/kg 14+3 days pre-surgery	Nivo. 3 mg/kg Q2W	neo+adj: 7.3 (5.4–7.9)	neo+adj: 4.1 (2.8–5.5)	↑Intratumoral immune cells ↑Chemokine transcripts ↑TCR clonal diversity
de Groot ¹³	15	0	Single arm, neo+adj	≤2x pembro. 200 mg, 21 days and 1 day pre-surgery	Pembro. 200 mg Q3W	neo+adj: 20.3 (8.6–28.5)	neo+adj: 4.5 (2.3–6.8)	Abundant CD68+ macrophages Very few T effector cells and immune activation markers
Ricardo McFaline-Figueroa [*]	25	0	Single arm, expansion, neo+adj	1x pembro. 200 mg 14+5 days pre-surgery	Pembro. 200 mg Q3W	neo+adj: 6.8 (NR)	neo+adj: 2.5 (NR)	↑T cell- and IFN γ -related transcripts ↓Cell cycle downregulation
Bagley [^]	16	0	Two arm, neo+adj (B1) vs neo+adj (B2)	B1: 1x reti. 500 mg + ragi. 300 mg + SRS† B2: 1x reti. 500 mg + ragi. 300 mg†	B1 and B2: reti. 500 mg Q4W + ragi. 300 mg Q2W	B1: 20.1 (NR) B2: 9.4 (NR) <i>p</i> =0.001	B1: 11.7 (NR) B2: 2.0 (NR) <i>p</i> =0.0002	↑Inflammatory cytokine responses ↑Proliferative T cell responses

^{*}Expansion cohort (Ricardo McFaline-Figueroa, J. *et al.* Neuro Oncol 2024, abstract no. CTIM-28) of Cloughesy 2019 study¹¹. [^]Bagley SJ, *et al.* J Clin Oncol 2023, abstract no. 2004.
[†]Length of neoadjuvant interval not reported. adj, adjuvant; Pts, patients; CI, confidence intervals; HR, hazard ratio; mo., months; mOS, median overall survival; mPFS, median progression-free survival; neo, neoadjuvant; New, newly diagnosed; nivo., nivolumab (anti-PD-1); NR, not reported; pembro., pembrolizumab (anti-PD-1); Q2W, every two weeks; Q3W, every three weeks; ragi., ragifilimab (anti-GITR); Rec., recurrent; reti., retifanlimab (anti-PD-1); SRS, stereotactic radiosurgery; TCR, T cell receptor.

Extended Data Table 2 | Whole-genome sequencing summary of the pretreatment specimen

Gene	Molecular findings	Metrics
<i>EGFR</i>	Focal amplification - chr7:52,854,346-55,496,211	27 copies
<i>MDM4</i>	Focal amplification - chr1:203,782,401-205,051,916	48 copies
<i>TERT</i>	Promoter hotspot mutation - chr5: g.1,295,113 G>A	25% AF
<i>PTEN</i>	Homozygous deletion - chr10:87,781,809-89,093,511	68% AF
<i>EGFR</i>	Intragenic deletion on chr7. Breakpoints at chr7:55,155,233 between ENST00000275493.6 exons 7 and 8, and chr7:55,160,268 within exon 12. Predicted effect: uncertain.	8% AF
<i>RB1</i>	Intrachromosomal rearrangement on chr13. Breakpoint at chr13:48,311,600 between ENST00000267163.4 exons 2 and 3. Predicted effect: Inactivation 1 of 1 gene copy.	85% AF
<i>RB1</i>	Intrachromosomal rearrangement on chr13. Breakpoint at chr13:48,320,255 between ENST00000267163.4 exons 2 and 3. Predicted effect: Inactivation 1 of 1 gene copy.	ND

AF, variant allele frequency; chr, chromosome; ND, not determined.

Extended Data Table 3 | Chronological details of the treatment schedule

Week	Day	Description	Details
1	+1	Cycle 1 of ICI	Nivolumab 480 mg plus relatlimab 160 mg Ipilimumab 80 mg
2	+13	Subtotal resection	
5	+35	First day of Rx	30x (daily) at 60Gy
6	+47	Cycle 2 of ICI	Nivolumab 480 mg
10	+75	Cycle 3 of ICI	Nivolumab 480 mg plus relatlimab 160 mg
	+76	Last day of Rx	30x (daily) at 60Gy
13	+91	Dose 1 of Vx	Personalized peptide vaccine*
	+95	Cycle 4 of ICI	Ipilimumab 80 mg
15	+105	Dose 2 of Vx	Personalized peptide vaccine
	+109	Cycle 5 of ICI	Nivolumab 480 mg plus relatlimab 160 mg
16	+118	Dose 3 of Vx	Personalized peptide vaccine
17	+119	Cycle 6 of ICI	Ipilimumab 80 mg
18	+132	Dose 4 of Vx	Personalized peptide vaccine
19	+138	Cycle 7 of ICI	Nivolumab 480 mg plus relatlimab 160 mg Ipilimumab 80 mg
21	+147	Dose 5 of Vx	Personalized peptide vaccine
23	+161	Dose 6 of Vx	Personalized peptide vaccine
24	+169	Cycle 8 of ICI	Nivolumab 480 mg plus relatlimab 160 mg
25	+181	Cycle 9 of ICI	Ipilimumab 80 mg
28	+202	Cycle 10 of ICI	Nivolumab 480 mg plus relatlimab 160 mg Ipilimumab 80 mg
30	+211	Dose 7 of Vx	Personalized peptide vaccine
33	+235	Cycle 11 of ICI	Nivolumab 480 mg plus relatlimab 160 mg Ipilimumab 80 mg
37	+263	Cycle 12 of ICI	Nivolumab 480 mg plus relatlimab 160 mg Ipilimumab 80 mg
42	+301	Dose 8 of Vx	Personalized peptide vaccine
46	+326	Cycle 13 of ICI	Nivolumab 480 mg plus relatlimab 160 mg
50	+354	Cycle 14 of ICI	Nivolumab 480 mg plus relatlimab 160 mg
57	+400	Dose 9 of Vx	Personalized peptide vaccine
78	+551	Dose 10 of Vx	Personalized peptide vaccine

*Personalized peptide vaccine administered to 78 weeks in 10 doses (Planned schedule: Q2W for the first 6 doses, Q4W for dose 7, Q12W for doses 8 and 9, and Q24W for dose 10). ICI, immune checkpoint inhibitor; Rx, radiotherapy; Vx, vaccine therapy.

Extended Data Table 4 | Normalized Olink proteomics plasma data expressed as normalized expression units on a log₂ scale

Protein	PRE		POST		log ₂ FC	log ₂ FC
	Day -4	Day +7	Day +12	POST (+7) – PRE (-4)	POST (+12) – PRE (-4)	
AXIN1	0.25	3.15	1.81	2.90	1.56	
BACH1	0.67	2.07	1.70	1.40	1.03	
BANK1	0.48	3.91	2.53	3.43	2.05	
BCR	0.14	2.23	1.31	2.09	1.17	
CDKN1A	-0.46	2.11	1.03	2.57	1.49	
CES3	1.18	0.14	-0.29	-1.04	-1.47	
CLIP2	0.34	3.24	2.39	2.90	2.05	
CXCL10	-0.51	0.96	3.22	1.47	3.73	
CXCL9	-0.84	1.11	2.91	1.95	3.75	
FOXO1	0.51	2.17	1.74	1.66	1.23	
GCG	-2.13	2.56	-0.78	4.69	1.35	
GOPC	0.58	3.04	1.82	2.46	1.24	
HBEGF	-1.82	0.23	-0.09	2.05	1.73	
ICA1	0.02	1.82	1.34	1.80	1.32	
IFNG	-0.11	3.04	6.00	3.15	6.11	
IKBKG	0.43	2.68	2.01	2.25	1.58	
IL10	0.91	3.02	5.9	2.11	4.99	
IL12A_IL12B	0.28	1.77	3.35	1.49	3.07	
IL12B	0.15	1.23	2.20	1.08	2.05	
IL1B	-0.54	0.62	1.25	1.16	1.79	
IL5	-1.69	0.38	-0.42	2.07	1.27	
IL6	-3.17	-0.64	2.14	2.53	5.31	
INPPL1	0.04	3.21	2.10	3.17	2.06	
IRAK4	0.56	3.34	1.78	2.78	1.22	
LAG3	0.03	3.67	4.93	3.64	4.9	
MGMT	-1.19	1.16	0.07	2.35	1.26	
MMP12	-0.71	0.43	1.35	1.14	2.06	
NFATC1	0.27	2.74	1.47	2.47	1.20	
NPY	-0.40	1.70	1.00	2.10	1.40	
NTF3	0.67	-0.62	-0.96	-1.29	-1.63	
NUB1	0.23	1.6	1.45	1.37	1.22	
PDCD1	-0.10	2.84	3.84	2.94	3.94	
PPP1R12A	0.68	2.72	2.07	2.04	1.39	
PPP1R9B	0.52	2.14	1.88	1.62	1.36	
PRKRA	0.07	1.48	1.41	1.41	1.34	
PSIP1	-0.14	1.16	1.10	1.30	1.24	
PTPN6	0.54	2.26	1.76	1.72	1.22	
S100A12	0.19	1.43	1.50	1.24	1.31	
SH2B3	0.23	3.47	1.95	3.24	1.72	
SMOC1	-1.01	1.02	1.15	2.03	2.16	
SPRY2	-0.34	0.87	0.90	1.21	1.24	
TANK	0.63	1.88	1.73	1.25	1.10	
TP53	-0.58	1.13	0.81	1.71	1.39	
TRIM5	-0.27	1.68	1.01	1.95	1.28	

Pre-treatment (Day -4) and post-treatment (Day +7 and +12) plasma samples collection time points shown relative to neoadjuvant immune checkpoint inhibitor (ICI) therapy initiation (Day +1). Proteins showing a >2-fold change at Day +7 and Day +12 are shown. FC, fold change.

Reporting Summary

Nature Portfolio wishes to improve the reproducibility of the work that we publish. This form provides structure for consistency and transparency in reporting. For further information on Nature Portfolio policies, see our [Editorial Policies](#) and the [Editorial Policy Checklist](#).

Statistics

For all statistical analyses, confirm that the following items are present in the figure legend, table legend, main text, or Methods section.

n/a Confirmed

- The exact sample size (n) for each experimental group/condition, given as a discrete number and unit of measurement
- A statement on whether measurements were taken from distinct samples or whether the same sample was measured repeatedly
- The statistical test(s) used AND whether they are one- or two-sided
Only common tests should be described solely by name; describe more complex techniques in the Methods section.
- A description of all covariates tested
- A description of any assumptions or corrections, such as tests of normality and adjustment for multiple comparisons
- A full description of the statistical parameters including central tendency (e.g. means) or other basic estimates (e.g. regression coefficient) AND variation (e.g. standard deviation) or associated estimates of uncertainty (e.g. confidence intervals)
- For null hypothesis testing, the test statistic (e.g. F , t , r) with confidence intervals, effect sizes, degrees of freedom and P value noted
Give P values as exact values whenever suitable.
- For Bayesian analysis, information on the choice of priors and Markov chain Monte Carlo settings
- For hierarchical and complex designs, identification of the appropriate level for tests and full reporting of outcomes
- Estimates of effect sizes (e.g. Cohen's d , Pearson's r), indicating how they were calculated

Our web collection on [statistics for biologists](#) contains articles on many of the points above.

Software and code

Policy information about [availability of computer code](#)

Data collection

Software used for data collection included: OncoPrint TCR Pan-Clonality Assay using Torrent Suite software version 5.18.1. TCR data analysis was performed in R version 4.3.0 (2023-04-21) using RStudio version 4.3.0 (with the following R packages; tidyverse version 2.0.0 ggpubr, ggsci version 3.0.0, lemon version 0.4.9, and UpSetR version 1.4.0, dplyr, cumsum function from base R). CTC image files were analyzed by CyteMapper v3.11.2.40, RareCyte). PhenoCycler-Fusion T cell quantification was performed utilizing HALO AI 3.6 with default AI-based cell sequencing and manual gating of T cell phenotypes. Subsequent broad immunophenotyping was performed with cell segmentation within StarDist using the DAPI channel (cytoplasm segmentation was estimated by morphological dilation of 5 μ m), and cell phenotyping for CD4+ and CD8+ T cells was performed using the machine learning classifier in QuPath v0.4.4. Cell neighborhood enrichment analysis was performed using a graph-based connectivity algorithm with the squidpy Python package. Flow cytometry samples were analyzed with FlowJo software v10.8 (BD Biosciences). WGS was performed using the Illumina NovaSeq 6000 platform. Clinical Genomics Analysis Platform was used to perform genome alignment (hg38) and variant calling using DRAGEN3.9, copy number variation using PURPLE, and structural rearrangement detection via DRAGEN SV and breakpointinspector packages. Total RNA samples were used as input for the NanoString IO360Panel and run on the nCounter MAX/FLEX Prep Station and Digital Analyzer. RNA signature scoring utilised the R (version 4.2.0) package singscore (1.16.0)

Data analysis

Software used for data analysis included: Illumina DRAGEN Bio-IT Platform v3.9 and DRAGEN Structural Variant (SV) Caller, and Python (hartwigmedical/pipeline5; packages: PURPLE, breakpointinspector) for NGS and transcriptome analysis; FlowJo v10.8 (BD Biosciences) for flow cytometry data; HALO AI v3.6, StarDist, QuPath v0.4.4, and Python (package: Squidpy) for PhenoCycler-Fusion analysis; R v4.3.0 (2023-04-21) with RStudio v4.3.0 (packages: tidyverse, ggpubr, ggsci, lemon, UpSetR) for OncoPrint TCR Pan-Clonality assay analysis; and CyteMapper Analysis Software Suite v3.11.2.40 (RareCyte) for CTC analysis.

For manuscripts utilizing custom algorithms or software that are central to the research but not yet described in published literature, software must be made available to editors and reviewers. We strongly encourage code deposition in a community repository (e.g. GitHub). See the Nature Portfolio [guidelines for submitting code & software](#) for further information.

Data

Policy information about [availability of data](#)

All manuscripts must include a [data availability statement](#). This statement should provide the following information, where applicable:

- Accession codes, unique identifiers, or web links for publicly available datasets
- A description of any restrictions on data availability
- For clinical datasets or third party data, please ensure that the statement adheres to our [policy](#)

Requests for data access will be reviewed by senior authors, and applicants can expect a response within two weeks of submission. Data will be provided under the following conditions: i) The research must have received ethical approval from a recognized ethics review board; ii) The request must align with the scientific aims and goals of the dataset; iii) The requesting team must demonstrate the ability to handle the data securely and responsibly; iv) A formal data usage agreement must be signed, ensuring the data will not be used for commercial purposes and will not be shared with unauthorized parties.

Research involving human participants, their data, or biological material

Policy information about studies with [human participants or human data](#). See also policy information about [sex, gender \(identity/presentation\), and sexual orientation](#) and [race, ethnicity and racism](#).

Reporting on sex and gender	The patient's biological sex and gender are both male, and both reported in the manuscript.
Reporting on race, ethnicity, or other socially relevant groupings	The patient's ethnicity/race is Caucasian, which is reported in the manuscript.
Population characteristics	One 56-year-old Caucasian Australian male.
Recruitment	The single patient was known to the primary author who conceived, designed, proposed, and administered the experimental neoadjuvant treatment regimen. The patient consented to participate in the n-of-one study, including the experimental treatment and collection and analysis of biospecimens.
Ethics oversight	This research was conducted in accordance with the Declaration of Helsinki. All drug therapy used in this study was obtained from Bristol-Myers Squibb, submitted to the Therapeutic Goods Administration, Australia (Special Access Scheme, Category A), and given with the consent of the patient. Biospecimen samples were acquired with consent from the Sydney Brain Tumour Bank (2019/ETH08929), the Melanoma Biospecimen Tissue Bank (HREC/11/RPAH/444), and the Macquarie University Cancer Biobank (HREC2793).

Note that full information on the approval of the study protocol must also be provided in the manuscript.

Field-specific reporting

Please select the one below that is the best fit for your research. If you are not sure, read the appropriate sections before making your selection.

- Life sciences Behavioural & social sciences Ecological, evolutionary & environmental sciences

For a reference copy of the document with all sections, see [nature.com/documents/nr-reporting-summary-flat.pdf](https://www.nature.com/documents/nr-reporting-summary-flat.pdf)

Life sciences study design

All studies must disclose on these points even when the disclosure is negative.

Sample size	This was a unique case study involving a single patient (N=1) who was known to the authors prior to presentation and diagnosis of glioblastoma. Treatment began within two weeks of diagnosis. The value of longitudinal biospecimens in the setting of neoadjuvant immunotherapy was well-known to the primary author; hence, while this is a descriptive case study of the management of a single patient, biospecimen collection (including blood and tumor tissue) and analysis for immune changes were integrated with clinical management from the beginning. This allowed us to perform several hypothesis-generating analyses. Including more patients was not feasible, nor appropriate. A clinical trial to test this regimen in a larger cohort is currently being designed at the Peter MacCallum Cancer Centre, in Melbourne, VIC, Australia.
Data exclusions	There were no data exclusions.
Replication	There were no technical replicates in the study, given the limited and irreplaceable biospecimens that required fractionation with different processing methods (e.g., tumor dissociates, fresh frozen tissue, FF/PE, etc).
Randomization	As this was a single patient study (N=1), no randomization was performed.
Blinding	The study was open-label and non-comparative. There was no blinding of any persons involved in the study, including the patient.

Reporting for specific materials, systems and methods

We require information from authors about some types of materials, experimental systems and methods used in many studies. Here, indicate whether each material, system or method listed is relevant to your study. If you are not sure if a list item applies to your research, read the appropriate section before selecting a response.

Materials & experimental systems

n/a	Involved in the study
<input type="checkbox"/>	<input checked="" type="checkbox"/> Antibodies
<input checked="" type="checkbox"/>	<input type="checkbox"/> Eukaryotic cell lines
<input checked="" type="checkbox"/>	<input type="checkbox"/> Palaeontology and archaeology
<input checked="" type="checkbox"/>	<input type="checkbox"/> Animals and other organisms
<input checked="" type="checkbox"/>	<input type="checkbox"/> Clinical data
<input checked="" type="checkbox"/>	<input type="checkbox"/> Dual use research of concern
<input checked="" type="checkbox"/>	<input type="checkbox"/> Plants

Methods

n/a	Involved in the study
<input checked="" type="checkbox"/>	<input type="checkbox"/> ChIP-seq
<input type="checkbox"/>	<input checked="" type="checkbox"/> Flow cytometry
<input type="checkbox"/>	<input checked="" type="checkbox"/> MRI-based neuroimaging

Antibodies

Antibodies used

Flow cytometry:

- CD45 BUV737; 1:200; clone HI30, Cat. 748719; BD Biosciences; RRID AB_2873123
- CD45RA BUV737; 1:100; clone HI100, Cat. 564442; BD Biosciences; RRID AB_2738810
- CD45RO BUV395; 1:20; clone UCHL1, Cat. 564291; BD Biosciences; RRID AB_2744410
- CD3 PE-CF594; 1:100; clone UCHT1, Cat. 562280; BD Biosciences; RRID AB_11153674
- CD3 BV786; 1:100; clone UCHT1, Cat. 565491; BD Biosciences; RRID AB_2739260
- HLA-DR, DP, DQ BUV395; 1:200; clone Tu39, Cat. 740302; BD Biosciences; RRID AB_274004
- CD8 V500; 1:100; clone SK1, Cat. 561617; BD Biosciences; RRID AB_10896281
- CD134 PE-Cy7; 1:20; clone Ber-ACT35, Cat. 563663; BD Biosciences; RRID AB_2738358
- HLA-A, B, C AF700; 1:80; clone W6/32, Cat. 311438; BioLegend; RRID AB_2566306
- CD4 AF700; 1:40; clone A161A1, Cat. 357418; BioLegend; RRID AB_2616933
- HLA-DR FITC; 1:100; clone L243, Cat. 307604; BioLegend; RRID AB_314682
- CD223 PE; 1:11; clone REA351, Cat. 130-105-452, Miltenyi Biotech; RRID AB_2656407
- Fc block 1:200; clone Fc1, Cat. 564220; BD Biosciences; RRID AB_2728082
- Human IgG4Fc PE; 1:100; clone HP6025, Cat. 9200-09; Southern Biotech; RRID AB_2796693
- CD279 BV421; 1:50; clone EH12.1; Cat. 562516; BD Biosciences; RRID AB_11153482
- FOXP3 PE-CF594; 1:20; clone 236A/E7; Cat. 563955; BD Biosciences; RRID AB_2738507
- GFAP AF488; 1:20; clone 1B4; Cat. 560297; BD Biosciences; RRID AB_1645350
- Granzyme B AF700; 1:100; clone GB11; Cat. 560213; BD Biosciences; RRID AB_1645453
- SOX2 PE; 1:100; clone O30-678; Cat. 562195; BD Biosciences; RRID AB_10895118
- CD152 APC; 1:20; clone 14D3; Cat. 17-1529-42; ThermoFisher Scientific; RRID AB_2688162
- KI-67 APC; 1:150; clone 20Raj1; Cat. 17-5699-42; ThermoFisher Scientific; RRID AB_2573218

PhenoCycler-Fusion:

- CD14 BX037; 1:200; clone AKYP0079, Cat. 4450047; Akoya Biosciences; RRID AB_3083457
- CD11c BX024; 1:400; clone AKYP0051, Cat. 4550114; Akoya Biosciences; RRID AB_3083459
- CD141 BX087; 1:200; clone AKYP0124, Cat. 4250097; Akoya Biosciences; RRID AB_3082975
- CD3e BX045; 1:200; clone AKYP0062, Cat. 4550119; Akoya Biosciences; RRID AB_2936080
- CD8 BX026; 1:200; clone AKYP0028 C8/114B, Cat. 4250012; Akoya Biosciences; RRID AB_2915960
- CD4 BX003; 1:200; clone AKYP0048 EPR6855, Cat. 4550112; Akoya Biosciences; RRID AB_3094499
- S100B BX049 (self-conjugated); 1:200; clone E7C3A, Cat. 423975F; Cell Signalling Technology

Circulating tumor cells:

- GFAP AF488; 1:50; clone 1B4, Cat. 560297; BD Pharmingen; RRID AB_1645350
- GFR PE; 1:100; clone Hu1; Cat. FAB9577P; R&D Systems; RRID AB_2942015
- CD45 AF750; 1:100; clone HI30; Cat. NBP1-79127AF750; Novus Biologicals; RRID AB_309771
- CEACAM-8/CD66b AF750; 1:100; clone 913542; Cat. FAB4246S; R&D Systems; RRID AB_3097716

We used healthy donors peripheral blood cells and glioblastoma tumor dissociates and cell lines to confirm the staining specificity and determine dilutions.

Validation

Antibodies 1 through 21 were validated by the relevant manufacturer as human-reactive (CQ testing or routinely tested) for application in flow cytometry. Additional manufacturer information: 9. Verified reactivity in human, cynomolgus, rhesus. 11. Verified reactivity in human, cynomolgus, rhesus. 17. Application "bioimaging". 20. Reactivity in human and rhesus. 21. Reactivity in human and dog. Antibodies 22 through 27 were developed by the manufacturer specifically for use in PhenoCycler-Fusion (PhenoCode Discovery) with human-reactivity. Antibody 28 is a carrier-free primary antibody validated as reactive in humans, mice, and rats by the manufacturer. It is designed for conjugation with fluorophores, metals, lanthanides, and oligonucleotides. The antibody was conjugated in-house to BX049 AlexaFluor 750 for PhenoCycler. Antibodies 29 through 32 were validated as human-reactive for bioimaging (29, 31) and/or flow cytometry (30, 32).

Flow Cytometry

Plots

Confirm that:

- The axis labels state the marker and fluorochrome used (e.g. CD4-FITC).
- The axis scales are clearly visible. Include numbers along axes only for bottom left plot of group (a 'group' is an analysis of identical markers).
- All plots are contour plots with outliers or pseudocolor plots.
- A numerical value for number of cells or percentage (with statistics) is provided.

Methodology

Sample preparation

Viable cryopreserved tumor or PBMC samples were thawed, washed and immediately stained with fluorophore-conjugated antibodies. Non-specific staining was blocked with Fc block. For the detection of T-cell bound nivolumab, cells were incubated with human IgG4Fc-PE. For indirect PD1 detection, samples were incubated with pembrolizumab (20µg/ml, Merck) prior to staining with fluorophore-conjugated antibodies, and cell-bound drugs (both IgG4) were detected with IgG4Fc-PE. For direct PD1 detection, cells were stained with CD279-BV421. Cell viability was determined by staining cells with LiveDead near-infrared (NIR) fixable dye. After cell surface staining, cells were fixed and permeabilized using the eBioscience transcription factor buffer kit, and stained with antibodies against intracellular markers plus Fc block in permeabilization buffer. Samples were washed extensively and immediately acquired on the flow cytometer.

Instrument

5-laser BD LSRFortessa X20 flow cytometer (BD Biosciences)

Software

FlowJo v10.8 (BD Biosciences)

Cell population abundance

No cell sorting was performed in this study

Gating strategy

The gating strategy involved: an FSC vs SSC gate to exclude debris, a time gate to exclude electronic noise, a viability gate (LiveDead NIR-negative) to exclude dead cells, a singlet gate (FSC height vs FSC area) to exclude doublets, and tumor and immune fraction gates to define the cells of interest. Tumor cells (SOX2+) were further gated for the GFAP+ fraction and analyzed for MHC class I (HLA-A, B, C) and MHC class II (HLA-DR, DP, DQ) expression. Tumor-infiltrating CD45+ (immune) fraction was analyzed for T cell content (CD3+), T cell subsets (CD8+ T, CD4+FOXP3- Tem and CD4+FOXP3+ Tregs) and immune checkpoints (CD39, LAG3, TIGIT, TIM3, and CTLA4).

GBM cells: CD45- _SSC-A int to high_SOX2+ _GFAP+.

TILs: CD45+ _SSC-A low_CD3+.

CD8 effector/memory cells: CD45+ _CD3+ SSC-A low_CD8+ _CD45RA- CD45RO+.

CD4 effector/memory cells: CD45+ _CD3+ SSC-A low_CD4+FOXP3- _CD45RA- CD45RO+.

Tregs: CD45+ _CD3+ SSC-A low_CD4+FOXP3+ _CD45RA-CD45RO+

- Tick this box to confirm that a figure exemplifying the gating strategy is provided in the Supplementary Information.

Magnetic resonance imaging

Experimental design

Design type

MRI Brain. Note that MRI was used as a routine diagnostic and monitoring tool, and was not experimental.

Design specifications

Brain Tumour Protocol

Behavioral performance measures

Nil

Acquisition

Imaging type(s)

MRI brain, with Siemens Healthineers MAGNETOM Vida

Field strength

3 Tesla

Sequence & imaging parameters

3D T2 FLAIR, 3D T1 MPRAGE, 3D MPRAGE C+, Ax T2, DWI, SWI, DSC Perfusion

Area of acquisition

Head - brain

Diffusion MRI

Used

Not used

Parameters

Nil

Preprocessing

Preprocessing software	Siemens
Normalization	Siemens Inline
Normalization template	Siemens Inline
Noise and artifact removal	Siemens Inline
Volume censoring	Siemens Inline

Statistical modeling & inference

Model type and settings	Dynamic Susceptibility Contrast
Effect(s) tested	Perfusion - CBV
Specify type of analysis:	<input checked="" type="checkbox"/> Whole brain <input type="checkbox"/> ROI-based <input type="checkbox"/> Both
Statistic type for inference	Perfusion Metrics
(See Eklund et al. 2016)	
Correction	Nil

Models & analysis

n/a	Involvement in the study
<input checked="" type="checkbox"/>	<input type="checkbox"/> Functional and/or effective connectivity
<input checked="" type="checkbox"/>	<input type="checkbox"/> Graph analysis
<input checked="" type="checkbox"/>	<input type="checkbox"/> Multivariate modeling or predictive analysis